Master's thesis
Theoretical physics

Validating the test-field method with mean-field dynamo simulations

Simo Tuomisto

December 2, 2019

Supervisor(s): Doc. Maarit Käpylä

Examiner(s): Prof. Kari Rummukainen
Doc. Maarit Käpylä

University of Helsinki
Faculty of Science

PL 64 (Gustaf Hällströmin katu 2a)
00014 Helsingin yliopisto

HELSINGIN YLIOPISTO — HELSINGFORS UNIVERSITET — UNIVERSITY OF HELSINKI

Tiedekunta — Fakultet — Faculty	Koulutusohjelma — Utbildningsprogram — Degree programme
Faculty of Science	Theoretical physics

Tekijä — Författare — Author

Simo Tuomisto

Työn nimi — Arbetets titel — Title

Validating the test-field method with mean-field dynamo simulations

Työn laji — Arbetets art — Level	Aika — Datum — Month and year	Sivumäärä — Sidantal — Number of pages
Master's thesis	December 2, 2019	72

Tiivistelmä — Referat — Abstract

The solar dynamo is a highly complex system where the small-scale turbulence in the convection zone of the Sun gives rise to large-scale magnetic fields. The mean-field theory and direct numerical simulations (DNSs) are widely used to describe these dynamo processes.

In mean-field theory the small-scale and large-scale fields are separated into a fluctuating field and a mean field with their own characteristic length scales. The evolution of the mean fields is governed by the contributions of fluctuating fields and these contributions are often written as so-called turbulent transport coefficients (TTCs). Thus obtaining accurate values for these coefficients is important for the evaluation of mean-field models. Recently, test-field method (TFM) has been used to obtain TTCs from DNSs.

The aim of this work is to use mean-field dynamo simulations to validate a test-field module (TFMod), which is an implementation of TFM. Both the TFMod and a mean-field module (MFMod), which is used to calculate the mean-field simulations, are written as modules in Pencil Code, which is a versatile magnetohydrodynamics simulation software.

The validation is done by comparing magnetic fields generated using DNS with magnetic fields generated using a mean-field simulation that uses TTCs obtained using the TFMod. In addition the TTCs measured by the TFMod are compared against expected values that are calculated using the second-order correlation approximation (SOCA). The model chosen for this validation is an α^2-dynamo driven by helical forcing as described by Mitra et al. (2010). The accuracy of the MFMod is confirmed by replicating mean-field models by Krause and Rädler (1980), Steenbeck and Krause (1969) and Jouve et al. (2008).

The measured TTCs replicate various expected properties with the exception of the β-tensor, which does not appear to be isotropic. This finding was shown by Viviani et al. (2019) to be an artefact from the original TFM tensor decomposition. Using all TTCs the MFMod is able to replicate various features of the DNS such as the growth rate, oscillation period and the field configurations of the magnetic fields.

The validation gives credence to the usage of the TFMod for the measurement of TTCs from DNSs, but it also shows that mean-field simulations such as the one described here are important for testing the validity of the TTCs produced by the TFM. It also suggests that utilizing the combination of the TFM and mean-field simulations in conjunction with DNS on more complicated dynamos could be an area of interest for future research.

Avainsanat — Nyckelord — Keywords

mean-field theory, test-field method, magnetohydrodynamics, computational physics, Pencil Code

Säilytyspaikka — Förvaringsställe — Where deposited

Muita tietoja — Övriga uppgifter — Additional information

Acknowledgements

Tämä työ ei olisi valmistunut ilman useiden ihmisen apua ja tukea. Ensimmäiseksi haluaisin kiittää ohjaajaani tähtitieteen dosentti Maarit Käpylää, jonka ehdotuksesta lähdin tekemään tätä tutkielmaa. Hänen tarkka ohjauksensa ja tarjoamansa luottamus tekemiseeni auttoivat minua suunnattomasti ja ilman häntä tämä tutkielma ei varmastikaan olisi nähnyt päivänvaloa.

Haluaisin myös kiittää koko Aalto Yliopiston Astroinformatics-ryhmää hyvistä keskusteluista, joiden kautta sain ratkaistua monia ongelmia niin koodauksen kuin fysiikan tulkitsemisen osalta. Suuri kiitos myös Aalto Yliopiston Tietotekniikan laitokselle sekä Aalto Yliopiston Science-IT:lle, joissa vallitseva hyvä työilmapiiri ja esimiesteni kannustus mahdollisti tutkielmani tekemisen töitteni ohessa.

Tämän työn valmistumista auttoi merkittävästi rahoitus Aalto Yliopiston Astroinformatics-ryhmältä ja Wiipurilaisen osakunnan stipendisäätiöltä. Laskentaresurssien tarjoamisesta kiitos kuuluu Aalto Yliopiston Science-IT:lle ja CSC:lle.

Opintojeni aikana olen saanut todella paljon tukea perheeltäni ja ystäviltäni ja olen siitä äärimmäisen kiitollinen. Usein, kun koin tämän työn tekemisen liian kuormittavaksi, te kuuntelitte huoliani ja tarjositte minulle muuta tekemistä, joka vei pahimman terän stressiltäni.

Viimeiseksi haluaisin erikseen kiittää kumppaniani Suvia. Olet peruskallioni, jota vasten olen pystynyt rakentamaan tämänkin rakennelman. Kiitos, että olet elämässäni.

Contents

Abbreviations & Symbols

$\alpha, \beta, \gamma, \delta, \kappa$ Turbulent transport coefficients written in terms of covariant tensors

$\overline{\mathcal{E}}$ Vector of the mean electromotive force

$\overline{\mathbf{F}}, \mathbf{F}'$ Mean and fluctuating parts of a vector field **F**

DNS Direct numerical simulation

MEMF Mean electromotive force

MFMod Mean-field module

MHD Magnetohydrodynamic

rms Root-mean-square

SOCA Second order correlation approximation

TFM Test-field method

TFMod Test-field module

TTC Turbulent transport coefficient

Eins

Hier kommt die Sonne

Zwei

Hier kommt die Sonne

Drei

Sie ist der hellste Stern von allen

Vier

Hier kommt die Sonne

Rammstein - *Sonne* (excerpt)

Chapter 1

Introduction

Astronomy is perhaps the oldest human science. For millenia people have looked upon the stars and wondered about their nature. Of these stars the Sun is by far the most interesting as it is the closest to our planet and provides energy that has enabled life to grow on Earth. All cultures have observed it and had their own theories behind its existence, but these theories were complicated by observations of sunspots on its perfect fiery circle. These dark spots on Sun's photosphere are areas of powerful magnetic fields, where the flux density is high enough to inhibit convection, resulting in an opaque dark area. However, it took until 19th century that they were linked to Sun's magnetic activity.[1]

In the West sunspots became the centre of attention in the beginning of the 17th century through observations by Thomas Harriot, Christoph Scheiner and Johann and David Fabricius. Their existence was philosophically problematic with the prevailing Ptolemaic theory of Sun being perfect and static. Due to the increased interest caused by this contradiction and with the help of more powerful telescopes, detailed counting of sunspots was started. These records were used in many statistical discoveries throughout the 19th century.

In 1843 Schwabe observationally verified an empirical law that states that sunspot numbers vary cyclically with a period of 11 years. Carrington in turn discovered, in 1858, that during this cycle there exists a latitudial drift, where sunspots are born at higher latitudes and from there their birth places will migrate towards the equator. After measurements of solar magnetic field became possible in the beginning of the 20th century, it was also shown that the mean radial component of the solar magnetic field behaves in a similar fashion.[1]

In 1908, some three hundred years after telescopic observations of the Sun started, Hale formulated that the solar magnetic fields were indeed tied to sunspots. Soon after this Hale also found out that polarity of the magnetic field alternates between the sunspot cycles and as a result the radial component of the Sun's magnetic field has a composite period of 22 years. The 11-year cyclical pattern is usually shown in a "butterfly diagram", where the sunspot latitudes are plotted against time, shown in Figure 1.1. The name of the diagram comes from the characteristic butterfly shape. This strong empirical evidence of solar magnetic activity demanded a theoretical foundation, but it took until the second half of the 20th century before a plausible mechanism behind Sun's magnetic field was formulated.[1, 2]

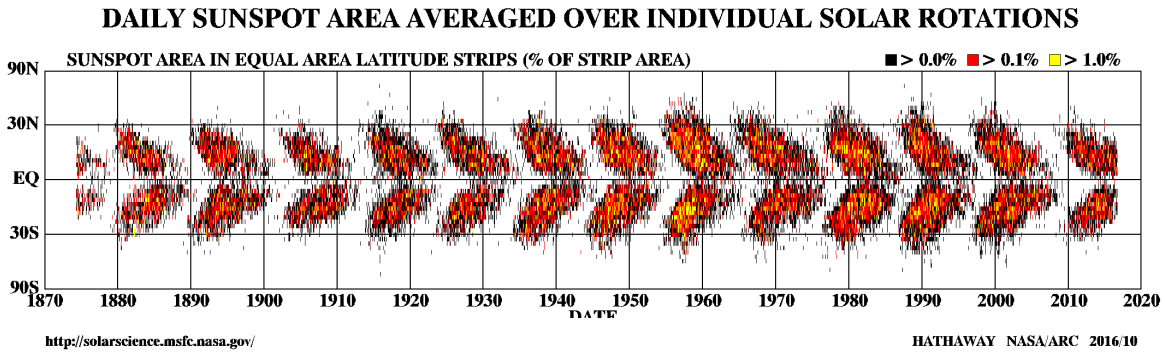

Figure 1.1: Butterfly diagram of daily sunspot area coverage. Source:[3]

In the 19th century it was postulated that solar magnetic field could be a remnant from the interstellar magnetic field that would have been amplified from a few microGauss strength to solar values by compression during the collapse of the molecular cloud wherefrom the Sun formed. This theory was quickly found out to be insufficient, as calculations showed that Ohmic decay would destroy the field in the convection zone in much shorter timescale than Sun's current lifetime. To solve this problem new methods needed to be invented.[1, 4]

Dynamo theory was suggested as a method of magnetic field generation by Larmor in 1919. According to this theory magnetic field was generated by the movement of charges in the convection zone plasma. A suitable movement of plasma across the field lines of a weak pre-existing magnetic field would result in the induction of a current parallel to the field. This induced current would then create a new magnified magnetic field perpendicular to it, which would again induce a current parallel to the initial magnetic field. Throughout this process both components of the magnetic field would grow in an exponential fashion to a macroscopic scale.[1, 5]

The applicability of the early dynamo theory took a hit in 1934, when Cowling proved his famous anti-dynamo theorem regarding axisymmetric fields. This theory showed that a steady axisymmetric magnetic field could not be maintained by dynamo action. The result was followed by other anti-dynamo theories which put further limits on the possible dynamo configurations. These problems were solved by postulating that the dynamo process is not a completely axisymmetric process, but instead a highly dynamical one, where small-scale magnetic field loops are generated and twisted by the rotationally affected convective turbulence. This small-scale induction will generate a mean electromotive force (MEMF), which will grow and amplify the magnetic field up to macroscopic scale in a process that resembles an inverse cascade. The dynamo cycle is completed by the large-scale stretching due to differential rotation, i.e. changing angular velocity in radius and latitude, of the Sun, generating zonal magnetic fields. This process then repeats itself in cyclic manner.[1, 6]

To build a quantitative physical model of this process, one would need a working turbulence theory of the solar convection zone. Unfortunately, such a theory does not exist. Hence, current theories are based on simplified attempts to describe turbulent convection. A common starting point for these theories is the *mean-field approach*. This theoretical framework assumes that key quantities, such as the velocity and magnetic fields, are composed of a slowly changing large-scale component and more rapidly changing small-scale component, obeying Reynolds' rules, which can be used to derive the equations for the mean fields. Under such procedure, the small-scale effects manifest themselves in the equations for the mean quantities in the form of turbulent correlations. The remaining, through extremely challenging task, is to find a proper description of those correlations. This is often done by assuming a priori information regarding the nature of the turbulence and only taking into account the velocity correlations of it up to a relevant order.

Through the mean-field approach the effects of turbulent motions in the convection zone are distilled into turbulent transport coefficients (TTCs), which contribute to the mean magnetic field through MEMF. This additional term arises in the *mean-field induction equation*, from which the mean magnetic fields can be solved with various analytical and numerical methods. Simplified forms of these coefficients and their properties, together with the differential rotation, are widely used to characterize different dynamo mechanisms within stars. Analytical methods using simplifying assumptions on the nature of the turbulence are often used to obtain the coefficients. Describing complex systems, however, is very problematic as the conditions required by the assumptions to be valid are only rarely met.[2, 6]

Today the advent of modern computers has allowed for direct numerical approaches. The

physics of the convection zone is often described by using a set of coupled differential equations that describe the evolution of density, temperature, velocity and magnetic fields, which are then solved with modern computational methods. However, the range of scales in the Sun makes solving these magnetohydrodynamic (MHD) equations computationally expensive. Due to this the models still roam on parameter regimes far from the real stars.

Test-field method (TFM) has recently been developed to measure TTCs numerically from MHD simulations. It has multiple advantages compared to analytical methods. Firstly, it does not require a priori information about the turbulence. Secondly, it is applicable in situations where the simplifying assumptions required by the analytical methods fail. Thirdly, it can be run at the same time as a full MHD simulation, thus providing an unique view to the data provided by the simulations. The ultimate goal of the TFM is to describe the dynamics of the MHD systems using the measured TTCs and the language of the mean-field theory.[7, 8]

In this work I present a mean-field module (MFMod) that has been integrated to Pencil Code, a high-order, fully compressible MHD solver. This new module solves the mean magnetic field based on the full set of TTCs, which can be generated analytically or by running a test-field module (TFMod) included in the Pencil Code during a MHD simulation. The validity of the MFMod is shown by reproducing results for several simple systems from literature.

Finally, the newly developed MFMod is run with the full TTCs obtained with the TFMod. By simulating a mean-field system using these coefficients and comparing the resulting fields to ones obtained from direct numerical simulation (direct numerical simulation (DNS)), the validity of both the TFMod and the limits of the mean-field approach are tested. The hope is that this combination of TFM and mean-field method will allow for better models of the solar dynamo. The simulation setup is visualized in Figure 1.2. This final simulation was also included in an article by Warnecke et al..[8]

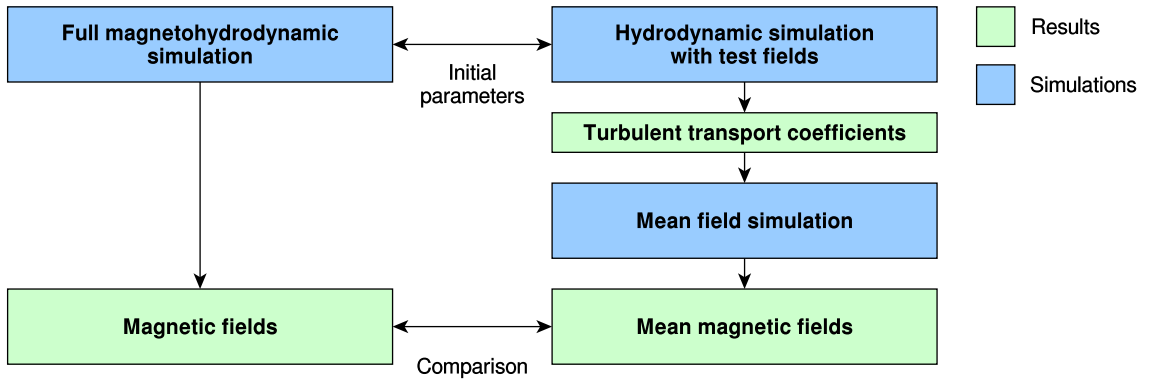

Figure 1.2: Simulations setup for test-field-simulation

Following this introduction Chapter 2 describes the structure of the Sun and the origin of the stellar magnetism. Chapter 3 goes through the basis of the mean-field theory and describes how the TTCs can be obtained using analytical methods. Chapter 4 in turn describes how the TFM works. After that Chapter 5 describes the design choices and the implementation of the MFMod. Chapter 6 goes through setups and results of five distinct mean-field simulations done with the simulation code. Each of the first four simulations test different aspects of the solver for validity, whereas the fifth simulation uses coefficients obtained using the TFM and compares the results with a full MHD simulation. This work ends with Chapter 7 where future applications of the code are discussed.

Chapter 2

Origin of Stellar Magnetism

Hydrodynamics of the convection zone

Sun's magnetic field is created through dynamo action that is driven by the turbulent motions of the convection zone. To understand this process one first needs to understand what drives the convection and the type of flows it exhibits.

Solar convection is driven by the energy generated in the solar core. In Sun's center the enormous gravitational pressure exerted by the outer layers result in a temperature that is high enough to start fusion reactions. In these reactions protons combine into deuterium, hydrogen's heavier isotope, that will in turn fusion with an additional proton forming helium-3 and releasing energy through gamma radiation and electron neutrinos. This proton-proton fusion releases 0.7 percent of the initial mass of the particles as energy and the resulting pressure from heat and radiation helps the Sun to counteract the gravitational pull that tries to collapse the star inwards. This process enables the Sun to be a stable star with a lifetime of billions of years. The high temperature causes matter to be fully ionized, while the enormous pressure results in a very short mean interaction time between ions and as a result, the core rotates as a continuous sphere of plasma.

The next layer radially outwards from the core, at around $R/R_\odot \approx 0.25$, is the radiative zone. In this region the temperature is not high enough to drive fusion, but the material is still ionized. However, due to short mean free path, any photons traveling there are absorbed almost immediately and re-emitted to random directions. For a single photon it takes around 10^7 years of random walking in order to climb to the top of the radiative zone. The energy transport is done though radiative diffusion and conduction until the bottom of

the convection zone at $R/R_\odot \approx 0.713$ is reached.[4, 9]

Between the radiative zone and the photosphere, from which photons finally escape to outer space, lies the convection zone. This area exhibits completely different dynamics compared to the inner regions. Firstly, the lower temperatures result in a drop in ionization. This causes material to appear opaque to radiation which reduces the efficiency of the radiative transport of energy. Now, due to *convective instability*, convection supersedes radiative diffusion and conduction as the preferred method of energy transport. Convective instability is defined through Schwarzschild criterion

$$\nabla > \nabla_{\text{ad}} \tag{2.1}$$

where

$$\nabla = \frac{\partial \ln T}{\partial \ln r} \tag{2.2}$$

is the logarithmic temperature gradient and ∇_{ad} is the adiabatic temperature gradient. In essence this equation tells that if the temperature gradient is higher than adiabatic one, excess thermal (kinetic) energy has to be transferred through movements of matter.

In convection hot material rises towards the surface while cold material sinks towards the core. Parcels of material heated by the excess energy have reduced density. This causes them to rise towards the surface until the pressure difference disappears. At the same time colder and denser material in the upper layers will fall towards the bottom layers. The distance travelled by a convective parcel of gas before dissolving is called the mixing length. Its scale is commonly assumed to be roughly equal to the pressure scale height

$$H_{\text{p}} = -\left(\frac{1}{p}\frac{\partial p}{\partial r}\right)^{-1} \tag{2.3}$$

By this assumption the mixing length is longer in the inner regions and shorter near the surface. Thus the scale of convective flows decreases from large-scale flows near the core to small-scale turbulent flows near the surface. Throughout this process the excess energy from the core is transported in a cascade from large-scale flows to the small-scale flows near the surface. This method of energy transport is very efficient and it results in highly turbulent flows, especially at the surface. It will also prove instrumental to the generation of the magnetic fields.[9, 10]

The matter in the convection zone acts as a viscous fluid. The kinematic viscosity ν and

conductivity σ of the plasma are often approximated using the Spitzer's equations:

$$\nu \approx \frac{\varepsilon_0^2 m_i^{1/2} (k_\mathrm{B} T)^{5/2}}{\rho Z^4 e^4 \ln \Lambda} \tag{2.4a}$$

$$\sigma \approx \frac{\varepsilon_0^2 (k_\mathrm{B} T)^{3/2}}{m_e^{1/2} Z e^2 \ln \Lambda} \tag{2.4b}$$

Here ε_0 is the vacuum permittivity, k_B is the Boltzmann constant, T is the temperature, m_i and m_e are the mass of the ions and electrons respectively, ρ is the ion density, e is the elementary charge, Z is the charge number of the ions and $\ln \Lambda$ is the Coulomb logarithm. The magnetic diffusivity η of the matter is then $\eta = c^2/(4\pi\sigma)$.[2, 9]

The strength of advection and induction in the convection zone are often measured in terms of dimensionless Reynolds numbers. Reynolds number $\mathrm{Re} = ul/\nu$ relates the relative velocity scale u and length scale l to the strength of kinematic viscosity to describe the vigor of convection. Magnetic Reynolds number $\mathrm{Re} = ul/\eta$ can in turn be used to estimate the strength of induction. In the Sun, where the convection is very strong and turbulent, the numbers are typically $\mathrm{Re} = \mathcal{O}(10^{12})$ and $\mathrm{Rm} = \mathcal{O}(10^{6})$. These values are extremely high and correspond to a very turbulent flow of matter with powerful induction of magnetic fields.[2, 9]

However, the turbulence is not isotropic as the Sun is rotating and the Coriolis force caused by rotation generates a preferred direction to the flows. These anisotropic small-scale motions can produce large-scale flows from a completely uniform initial state through so-called Reynolds stresses.[9]

The most pronounced manifestation of these flows is the difference in rotation rates between equatorial (faster) and polar (slower) regions. It has been dubbed *latitudinal differential rotation* and it is visible on the surface of the sun. Its name comes from the fact that the rotation profile of the convection zone is non-uniform when compared to the core. This non-uniformity is present throughout the convection zone, but it reaches its maximum at the top of the convection zone where Sun's polar regions exhibit a rotation period of around 30 days whereas near the equator the period is 25 days. At the bottom of the convection zone is a layer called the tachocline, below which the rotation turns to the uniform rotation of the core. The rotation rate profile of the convection zone at various latitudes is visualized in Figure 2.1.[9]

The preferred direction induced by rotation also affects the heat transport, which results

in a small temperature difference between the equator and the poles. Even though this temperature difference is small, it results in a baroclinic flows that are vital to *meridional circulation*, where the material rises near the equator, then travels towards the poles on the convection zone's upper layers and travels back to deeper regions near the poles. These two large-scale circulation patterns are linked to each other.[9]

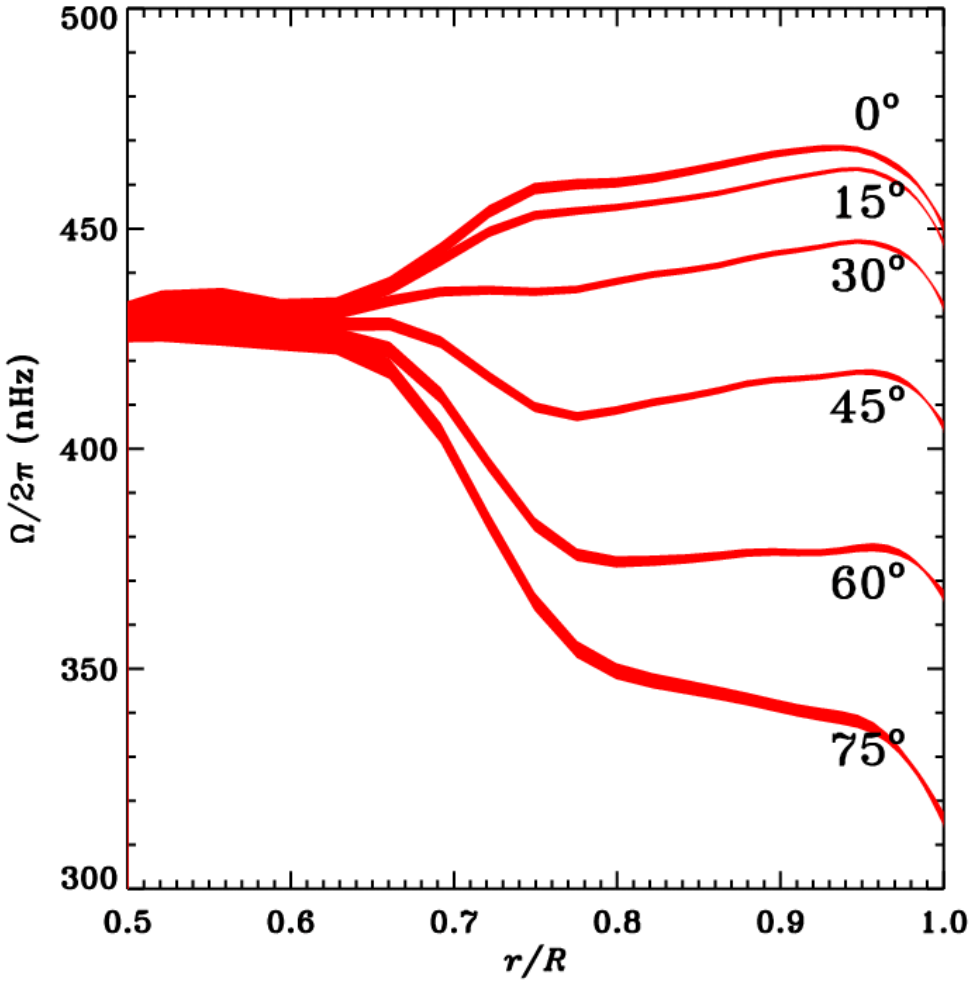

Figure 2.1: Rotation rate of the solar convection zone at various latitudes measured through helioseismology. Source:[11]

Dynamo processes in the convection zone

The previously described complex movement of ionized matter is the reason why Sun has a strong magnetic field that has been sustained at the high levels for a long timescale. Maxwell's equations tell that a current caused by movement of charged particles induces

a magnetic field. This effect is usually written in one equation by combining Maxwell's equations

$$\begin{cases} \boldsymbol{\nabla} \cdot \mathbf{E} = \dfrac{\rho}{\varepsilon_0} & \text{(2.5a)} \\ \boldsymbol{\nabla} \cdot \mathbf{B} = 0 & \text{(2.5b)} \\ \boldsymbol{\nabla} \times \mathbf{E} = -\dfrac{\partial \mathbf{B}}{\partial t} & \text{(2.5c)} \\ \boldsymbol{\nabla} \times \mathbf{B} = \mu_0 \mathbf{J} + \dfrac{1}{c^2} \dfrac{\partial \mathbf{E}}{\partial t} & \text{(2.5d)} \end{cases}$$

and Ohm's law

$$\mathbf{J} = \sigma \left(\mathbf{E} + \mathbf{u} \times \mathbf{B} \right) \tag{2.6}$$

into an *induction equation* that describes the evolution of magnetic fields.

Solving electrical field $\mathbf{E}$ from Ohm's law gives

$$\mathbf{E} = \eta \mu_0 \mathbf{J} - \mathbf{u} \times \mathbf{B} \tag{2.7}$$

where $\eta = (\sigma \mu_0)^{-1}$ is the magnetic diffusivity. Inserting this into Faraday's law of induction (Eq. 2.5c) gives

$$\frac{\partial \mathbf{B}}{\partial t} = \boldsymbol{\nabla} \times (\mathbf{u} \times \mathbf{B} - \eta \mu_0 \mathbf{J}) \tag{2.8}$$

which is the *induction equation*.[2]

The induction equation can be further simplified when the contribution of the time derivative part of electric field, also known as Faraday displacement current, in Eq. 2.5d is small. This occurs when the electrical field varies over a time scale larger than the Faraday time $\tau_{\text{Faraday}} = \eta / c^2$. In stars this condition is always satisfied and thus the term can be ignored.[2]

Under these conditions Eq. 2.5d reduces to Ampere's law

$$\boldsymbol{\nabla} \times \mathbf{B} = \mu_0 \mathbf{J} \tag{2.9}$$

and inserting this into the induction equation gives

$$\frac{\partial \mathbf{B}}{\partial t} = \boldsymbol{\nabla} \times (\mathbf{u} \times \mathbf{B}) - \eta \boldsymbol{\nabla} \times \boldsymbol{\nabla} \times \mathbf{B} \tag{2.10}$$

Now the double curl can be written as $\boldsymbol{\nabla} \times \boldsymbol{\nabla} \times \mathbf{B} = \boldsymbol{\nabla}(\boldsymbol{\nabla} \cdot \mathbf{B}) - \nabla^2 \mathbf{B}$, but as $\boldsymbol{\nabla} \cdot \mathbf{B} = 0$, it reduces into $\boldsymbol{\nabla} \times \boldsymbol{\nabla} \times \mathbf{B} = -\nabla^2 \mathbf{B}$. This give a different form for the induction equation

$$\frac{\partial \mathbf{B}}{\partial t} = \boldsymbol{\nabla} \times (\mathbf{u} \times \mathbf{B}) + \eta \nabla^2 \mathbf{B} \tag{2.11}$$

which is widely used in dynamo theory.[6, 7]

Certain dynamics of the induction equation, when combined with the knowledge of the hydrodynamics of the convection zone, are crucial to the dynamo action. In the convection zone, where the Reynolds number is huge, the magnetic field can be considered to be frozen to the fluid. Due to this, fields lines of magnetic field in the convection zone follow the motions of the plasma. It can be shown that in a diffusionless case the magnetic flux across any surface will be preserved by motion of the plasma. By following the motion of a surface S in the plasma one can create a *flux tube*. Shearing motions which increase the length of the flux tube or compress the surface S will increase the magnetic flux density $\mathbf{B}$, while twisting motions can change the direction of the magnetic field lines.[2]

In practice the freezing is limited by the turbulent diffusion, which reconnects field lines and breaks up the flux tubes. Nevertheless, fluid packages that rise from the bottom of the convection zone can contain magnetic fields from the radiative zone in form of flux tubes. Now the turbulent motions of the plasma on these rising and falling fluid packages can amplify and modify the magnetic field.[9]

First of these methods of magnetic field creation was proposed in 1955 by Parker in his highly influential paper, which marked the first steps towards mean-field magnetohydrodynamics. He proposed that the solar dynamo could operate thanks to helical motions caused by Coriolis force. These helical motions twist the magnetic field and as a result a MEMF, that is proportional to the *mean magnetic field*, would be created. This process was later named $\boldsymbol{\alpha}$-effect. The helical motion in the turbulence twists the originally toroidal loops to poloidal loops while also increasing the magnetic field strength. Similar effect converts the poloidal field into a toroidal one. However, at high field strengths this effect is quenched and the proportionality between the MEMF and the mean magnetic field becomes non-linear. A dynamo where both toroidal and poloidal fields are maintained by the $\boldsymbol{\alpha}$-effect is called a $\boldsymbol{\alpha}^2$-dynamo.[2, 9]

In the Sun $\boldsymbol{\alpha}$-effect is complemented by $\boldsymbol{\Omega}$-effect, which is related to the non-uniformity of the rotation profile. Rising poloidal magnetic fields are turned into toroidal fields when they encounter the shear lines resulting from the differential rotation. These processes together form a $\boldsymbol{\alpha\Omega}$-dynamo, where poloidal and toroidal fields are constantly transformed into each others. A mix between these two dynamos is a $\boldsymbol{\alpha^2\Omega}$-dynamo, where both $\boldsymbol{\alpha}$-effect and $\boldsymbol{\Omega}$-effect contribute to the toroidal field generation. All of these dynamos are also affected by turbulent diffusivity, also known as the $\boldsymbol{\beta}$-effect, which reconnects field lines and breaks down flux tubes.[2, 9, 12]

Some dynamos exhibit turbulent magnetic pumping, called the γ-effect, which is advection-like behavior caused by the turbulence. It expels magnetic fields from regions of high turbulence and thus it has also been called the turbulent diamagnetic effect.[2, 6, 9]

Systems with shear can also exhibit a Rädler-effect or shear-current effect. These contributions, often denoted with δ, can also contribute to dynamo processes, but these kinds of dynamos are beyond this work.[2]

After it was shown that magnetic fields can indeed be generated through turbulent dynamo action a mathematical framework to derive the contributions of the turbulence was needed. Nowadays this field of magnetohydrodynamics is known as mean-field magnetohydrodynamics or mean-field theory. Many of the effects discussed above were first described analytically using the framework provided by the mean-field theory.[2, 6]

Chapter 3

Mean-field theory

Basic assumptions of mean-field theory

Mean-field theory tries to predict the effects of turbulence on a quantity of interest as a function of relevant system parameters. By utilizing the mathematical framework provided by the theory, many important results were obtained at a time when large-scale simulations would have been completely unfeasible. This chapter, that introduces the basics of mean-field theory, follows roughly the treatment given in chapter four of a seminal book written by Krause and Rädler in 1980.[6]

A more recent treatment given in a review by Brandenburg and Subramanian (2005) is also used for reference.[2]

The basic premise of mean-field theory is that the fields of interest can be separated into two parts: a mean field and a fluctuating field. The mean field consists of an ensemble mean of a system with respect to some characteristic time and space scale. The choice of the scale is not arbitrary, but instead determined by the scale of the turbulence. In general when mean field varies in time or in space, it should do it slower and/or over larger scales than the turbulent motions. Thus there is *scale separation* between the mean field and fluctuating field. A mean part of vector field $\mathbf{F}$ will be denoted in the following chapters by overbar so that for $\mathbf{F}$ it would be $\overline{\mathbf{F}}$.

Whatever does not belong to the mean field, belongs to the fluctuating part of the field. This part consists of the fields' small-scale fluctuations that vary over scales that are much smaller than the ones of $\overline{\mathbf{F}}$, much faster than $\overline{\mathbf{F}}$. The fluctuating part of the field $\mathbf{F}$ will be

denoted in the following chapters by prime so that for $\mathbf{F}$ it would be $\mathbf{F}'$.

These fields should be complimented by an *averaging operator*, denoted by overbar. The choice of this averaging operator is arbitrary as long as it follows the Reynolds' rules:

$$\begin{aligned}
\mathbf{F} &= \overline{\mathbf{F}} + \mathbf{F}' & \overline{\overline{\mathbf{F}}} &= \overline{\mathbf{F}} \\
\overline{\mathbf{F}'} &= 0 & \overline{\mathbf{F} + \mathbf{G}} &= \overline{\mathbf{F}} + \overline{\mathbf{G}} \\
\overline{\overline{\mathbf{F}}\,\overline{\mathbf{G}}} &= \overline{\mathbf{F}}\,\overline{\mathbf{G}} & \overline{\overline{\mathbf{F}}\mathbf{G}'} &= 0 \\
\overline{\frac{\partial \mathbf{F}}{\partial t}} &= \frac{\partial \overline{\mathbf{F}}}{\partial t} & \overline{\frac{\partial \mathbf{F}}{\partial x_i}} &= \frac{\partial \overline{\mathbf{F}}}{\partial x_i}
\end{aligned} \tag{3.1}$$

Here $\overline{\mathbf{F}}$ ($\overline{\mathbf{G}}$) and $\mathbf{F}'$ ($\mathbf{G}'$) are now the mean and fluctuating parts of the field $\mathbf{F}$ ($\mathbf{G}$) respectively.

By using the averaging operator on the full equation of the field, one obtains an equation that consists only of mean fields and a coupling term that describes the mean effects of the fluctuating fields. Subtracting the mean-field equation from the original equation gives an analogous equation for the fluctuations. The equation of the fluctuating fields is coupled with the equation of the mean fields through various terms that describe the effects of the mean field on the fluctuations. In analytic treatments various simplifications are often used when solving these equations.

If one can solve the equation describing the fluctuations, the result can be used through the coupling to describe the effect of fluctuating fields on the mean fields. Thus the effect of small-scale fields can be found and by solving the mean-field equation, the large-scale fields can be obtained.

Mean-field induction equation

The mathematical framework of mean-field theory can be used for arbitrary fields, but in the case of solar magnetohydrodynamics, the goal is to understand the presence of large scale magnetic fields. As mentioned in section 2.2, the dynamo processes in the solar

convection zone can be described through the induction equation (Eq. (2.8)

$$\frac{\partial \mathbf{B}}{\partial t} = \boldsymbol{\nabla} \times (\mathbf{u} \times \mathbf{B} - \eta\mu_0 \mathbf{J}) \tag{3.2}$$

where the relevant fields are magnetic field, velocity field and current density. Hence the emphasis is to turn this equation as a mean-field equation.

By applying the substitutions $\mathbf{B} = \overline{\mathbf{B}} + \mathbf{B}'$, $\mathbf{u} = \overline{\mathbf{u}} + \mathbf{u}'$ and $\mathbf{J} = \overline{\mathbf{J}} + \mathbf{J}'$ the equation turns into

$$\frac{\partial \mathbf{B}'}{\partial t} - \boldsymbol{\nabla} \times \left(\overline{\mathbf{u}} \times \mathbf{B}' - \mathbf{u}' \times \overline{\mathbf{B}} - \mathbf{u}' \times \mathbf{B}' + \eta\mu_0 \mathbf{J}'\right) = \tag{3.3}$$

$$-\frac{\partial \overline{\mathbf{B}}}{\partial t} + \boldsymbol{\nabla} \times \left(\overline{\mathbf{u}} \times \overline{\mathbf{B}} - \eta\mu_0 \overline{\mathbf{J}}\right) \tag{3.4}$$

The mean field part of this equation can be obtained by applying the averaging operator to the equation and using Reynolds relations to simplify the result. This gives the equation

$$\frac{\partial \overline{\mathbf{B}'}}{\partial t} - \boldsymbol{\nabla} \times \left(\overline{\overline{\mathbf{u}} \times \mathbf{B}'} - \overline{\mathbf{u}' \times \overline{\mathbf{B}}} - \overline{\mathbf{u}' \times \mathbf{B}'} + \eta\mu_0 \overline{\mathbf{J}'}\right) = \tag{3.5}$$

$$-\frac{\partial \overline{\overline{\mathbf{B}}}}{\partial t} + \boldsymbol{\nabla} \times \left(\overline{\overline{\mathbf{u}} \times \overline{\mathbf{B}}} - \eta\mu_0 \overline{\overline{\mathbf{J}}}\right) \tag{3.6}$$

which can be simplified to give the *mean-field induction equation*

$$\frac{\partial \overline{\mathbf{B}}}{\partial t} = \boldsymbol{\nabla} \times \left(\overline{\mathbf{u}} \times \overline{\mathbf{B}} + \overline{\boldsymbol{\mathcal{E}}} - \eta\mu_0 \overline{\mathbf{J}}\right) \tag{3.7}$$

where $\overline{\boldsymbol{\mathcal{E}}} = \overline{\mathbf{u}' \times \mathbf{B}'}$. The field $\overline{\boldsymbol{\mathcal{E}}}$, that consists of mean effects of the turbulent fields, is now the coupling between the mean fields and the fluctuations. As it acts as an additional electromotive force inducing magnetic fields, it is called the mean electromotive force or turbulent electromotive force (MEMF).

Now the equation for the fluctuations of the magnetic field can be created by subtracting the mean-field induction equation from the original equation. The result is

$$\frac{\partial \mathbf{B}'}{\partial t} = \boldsymbol{\nabla} \times \left(\overline{\mathbf{u}} \times \mathbf{B}' + \mathbf{u}' \times \overline{\mathbf{B}} + \mathbf{G} - \eta\mu_0 \mathbf{J}'\right) \tag{3.8}$$

where $\mathbf{G} = \mathbf{u}' \times \mathbf{B}' - \overline{\boldsymbol{\mathcal{E}}}$.

When the assumption of small Faraday displacement current is made, the last term can be written as $\mu_0 \mathbf{J}' = \boldsymbol{\nabla} \times \mathbf{B}'$. After this change the equation shows that the fluctuation of magnetic field $\mathbf{B}'$ is some functional of $\overline{\mathbf{u}}$, $\mathbf{u}'$ and $\overline{\mathbf{B}}$. Thus knowledge of velocity fields and the mean magnetic field will determine the fluctuations of the magnetic fields.[13]

Solving the mean electromotive force

The equations defined previously can be written in a more mathematically rigorous form by defining two-point, two-time correlation tensors, that describe correlations between the different fluctuating fields.

Let Q,P and B be the a two-point, two-time correlation tensor for the fluctuating velocity field; fluctuating velocity field and fluctuating magnetic field; and fluctuating magnetic field respectively:

$$Q_{ij}(x,\xi,t,\tau) = \overline{\mathbf{u}'_i(x,t)\mathbf{u}'_j(x+\xi,t+\tau)} \tag{3.9}$$

$$P_{ij}(x,\xi,t,\tau) = \overline{\mathbf{u}'_i(x,t)\mathbf{B}'_j(x+\xi,t+\tau)} \tag{3.10}$$

$$B_{ij}(x,\xi,t,\tau) = \overline{\mathbf{B}'_i(x,t)\mathbf{B}'_j(x+\xi,t+\tau)} \tag{3.11}$$

In all of these tensors ξ and τ are some displacements of location and time near point (x,t).

In addition, let tensors

$$Q_{ijk}(x,\xi,\eta,t,\tau,\sigma) = \overline{\mathbf{u}'_i(x,t)\mathbf{u}'_j(x+\xi,t+\tau)\mathbf{u}'_k(x+\xi+\eta,t+\tau+\sigma)} \tag{3.12}$$

and

$$P_{ijk}(x,\xi,\eta,t,\tau,\sigma) = \overline{\mathbf{u}'_i(x,t)\mathbf{u}'_j(x+\xi,t+\tau)\mathbf{B}'_k(x+\xi+\eta,t+\tau+\sigma)} \tag{3.13}$$

be third rank correlation tensors, where η and σ are again displacements in place and time. This process can be continued for fourth, fifth, sixth etc. rank tensors.

Also let us denote correlation tensors P_{ij} and P_{ijk}, where the displacements are zero, with

$$p_{ij}(x,t) = P_{ij}(x,0,t,0) \tag{3.14}$$

$$p_{ijk}(x,\xi,t,\tau) = P_{ijk}(x,\xi,0,t,\tau,0) \tag{3.15}$$

Now the MEMF can be written as

$$\overline{\mathcal{E}}_i = \varepsilon_{ijk}p_{jk}(x,t) \tag{3.16}$$

By further defining two operators

$$D_{jn} = \left(\frac{\partial}{\partial t} - \eta\nabla^2\right)\delta_{jn} - \varepsilon_{jkl}\varepsilon_{lmn}\frac{\partial}{\partial x_k}\overline{\mathbf{u}}_m \tag{3.17}$$

$$D_{jmn} = \varepsilon_{jkl}\varepsilon_{lmn}\frac{\partial}{\partial x_k} \tag{3.18}$$

and writing the induction equation (2.11) as

$$\frac{\partial \mathbf{B}}{\partial t} - \eta \nabla^2 \mathbf{B} - \boldsymbol{\nabla} \times \mathbf{u} \times \mathbf{B} = 0 \tag{3.19}$$

$$\left(\frac{\partial}{\partial t} - \eta \nabla^2 \right) \mathbf{B} - \boldsymbol{\nabla} \times (\overline{\mathbf{u}} + \mathbf{u}') \times \mathbf{B} = 0 \tag{3.20}$$

$$\left(\frac{\partial}{\partial t} - \eta \nabla^2 \right) \mathbf{B} - \boldsymbol{\nabla} \times \overline{\mathbf{u}} \times \mathbf{B} = \boldsymbol{\nabla} \times \mathbf{u}' \times \mathbf{B} \tag{3.21}$$

This can be written in the component form

$$\left(\frac{\partial}{\partial t} - \eta \nabla^2 \right) B_j - \left(\boldsymbol{\nabla} \times \overline{\mathbf{u}} \times \mathbf{B} \right)_j = \left(\boldsymbol{\nabla} \times \mathbf{u}' \times \mathbf{B} \right)_j \tag{3.22}$$

$$\left(\frac{\partial}{\partial t} - \eta \nabla^2 \right) B_j - \varepsilon_{jkl} \varepsilon_{lmn} \frac{\partial}{\partial x_k} \overline{u}_m B_n = \varepsilon_{jkl} \varepsilon_{lmn} \frac{\partial}{\partial x_k} u'_m B_n \tag{3.23}$$

or

$$D_{jn} B_n = D_{jmn} u'_m B_n \tag{3.24}$$

Now using the averaging operator on this equation results in the mean-field induction equation:

$$D_{jn} \overline{B}_n = D_{jmn} p_{mn} \tag{3.25}$$

From the definition of D_{jmn} and the form of $\overline{\boldsymbol{\mathcal{E}}}$ given in Eq. (3.16), it is easy to see that the right side of the equation corresponds to $\boldsymbol{\nabla} \times \overline{\boldsymbol{\mathcal{E}}}$.

Changing coordinates from x and t to $x + \xi$ and $t + \tau$ in Eq. (3.24), taking derivatives with respect to ξ and τ, multiplying the whole equation with $u'_m(x,t)$ and finally taking the average results in equation

$$D_{jn} P_{mn} = D_{jmp} (Q_{mn} \overline{B}_p) + D_{jnp} p_{mnp} \tag{3.26}$$

This represents a differential equation for correlation P_{mn}, where a higher-order statistical moment p_{mnp} appears. Equations for higher moments can be found by repeating the same procedure, but as each equation has a tensor of a higher order, the system is an infinite series of differential equations. Thus, a suitable *closure* is required. By limiting the correlations of the turbulent velocity field $\mathbf{u}'$ (terms $Q_{ijk\ldots st}$) to a suitable precision, the equations for $P_{ijk..st}$ end at some order.

A famous and commonly used closure is the second-order correlation approximation (SOCA), also known as first-order smoothing approximation (FOSA). In this closure only second-order contributions of $\mathbf{u}'$ are taken into account and thus equations (3.25) and (3.26)

turn into

$$D_{jn}\overline{B}_n(x,t) = D_{jmn}p_{mn}(x,t) \tag{3.27a}$$
$$D_{jn}P_{mn}(x,\xi,t,\tau) = D_{jmp}(Q_{mn}(x,\xi,t,\tau)\overline{B}_p(x+\xi,t+\tau)) \tag{3.27b}$$

This approximation holds when

$$\min(\mathrm{Rm},\mathrm{St}) \ll 1 \tag{3.28}$$

where Rm and St are dimensionless parameters called *magnetic Reynolds number* and *Strouhal number*

$$\begin{aligned} \mathrm{Rm} &= \frac{u'_{\mathrm{rms}}\lambda_{corr}}{\eta} \\ \mathrm{St} &= \frac{\tau_{\mathrm{corr}}}{\tau_{\mathrm{turnover}}} \end{aligned} \tag{3.29}$$

where u'_{rms} is the root-mean-square (rms) value of the velocity fluctuation, λ_{corr} is the correlation length, τ_{corr} is the relaxation time over which fluctuations happen and $\tau_{\mathrm{turnover}} = l/u'_{\mathrm{rms}}$ is the turnover time over which eddies stay identifiable. These quantities describe how important advection is compared to diffusion and what is the ratio of representative timescale and the turbulent turnover time respectively. In stellar situations the values of Rm are typically very high, so applicability of SOCA depends largely on the value of St.[2, 9]

General solution for the MEMF in Eq. (3.27a), given turbulent velocity field $\mathbf{u}'$ and mean magnetic field $\overline{\mathbf{B}}$, can be obtained with Green's functions.

A Green's tensor G_{jk} for differential operator D_{jk} satisfies conditions

i. $G_{jp}(x,\xi,t,\tau) = 0$, if $t < \tau$

ii. $G_{jp}(x,\xi,t,\tau) \to 0$, if $|x-\xi| \to 0$

iii. $D_{jk}G_{kp}(x,\xi,t,\tau) = \delta_{jp}\delta(x-\xi,t-\tau)$, if $t > \tau$

and it can be used to create a Green's function kernel

$$K_{ij}(x,\xi,t,\tau) = \varepsilon_{imn}\varepsilon_{pqr}\varepsilon_{rsj}\frac{\partial G_{np}(x,x-\xi,t,t-\tau)}{\partial \xi_q}Q_{ms}(x,-\xi,t,-\tau) \tag{3.30}$$

Using the kernel K_{ij} the MEMF $\overline{\boldsymbol{\mathcal{E}}}$ can be integrated from

$$\overline{\mathcal{E}}_i(x,t) = \int\int K_{ij}(x,\xi,t,\tau)\overline{B}_j(x-\xi,t-\tau)\,d^3\xi\,d\tau \tag{3.31}$$

It is easy to see that equation depends only on $\mathbf{u}'$ and $\overline{\mathbf{B}}$.

A simpler form of the same result can be obtained by starting from the induction equation for the fluctuating magnetic field (Eq. (3.8))

$$\frac{\partial \mathbf{B}'}{\partial t} = \boldsymbol{\nabla} \times \left(\overline{\mathbf{u}} \times \mathbf{B}' + \mathbf{u}' \times \overline{\mathbf{B}} + \mathbf{G} - \eta \mu_0 \mathbf{J}' \right) \tag{3.32}$$

and arguing that

(a) $\overline{\mathbf{u}} \times \mathbf{B}'$ is relevant only in systems with strong shear, where it can cause shear-current effects.

(b) In the regime of low Strouhal numbers the non-linear term $\mathbf{G}$ is small.

(c) Magnetic diffusivity η is low, which means that the last term is small.

These conditions result in an equation

$$\frac{\partial \mathbf{B}'}{\partial t} = \boldsymbol{\nabla} \times \mathbf{u}' \times \overline{\mathbf{B}} \tag{3.33}$$

If this equation is integrated over time, crossed with $\mathbf{u}'$ and finally averaged with the averaging operator one obtains an equation for the MEMF:

$$\overline{\boldsymbol{\mathcal{E}}} = \overline{\mathbf{u}' \times \int \boldsymbol{\nabla} \times \mathbf{u}' \times \overline{\mathbf{B}} \, dt} \tag{3.34}$$

Covariant form of the mean electromotive force

Although the integral equation (3.31) can be used to calculate the MEMF, it is often of interest to study its structure. The two-scale approximation, already familiar from the basic mean-field approach principles, which assumes that mean fields and fluctuating fields act at different time and length scales, allows one to simplify the aforementioned equations. Condition for this approximation to be applicable is that either

$$\lambda_{corr} \ll \overline{\lambda} \tag{3.35}$$

or

$$\tau_{\text{corr}} \ll \overline{\tau} \tag{3.36}$$

holds. Here $\overline{\lambda}$ and $\overline{\tau}$ are the characteristic length and time scales of the mean fields respectively.

When this approximation holds the mean field is affected instantaneously by turbulent fields within a limited spatial region around the point of interest. This means that the mean magnetic field is a function of $x + \xi$ and t instead of $x + \xi$ and $t + \tau$. Additionally, one can represent the mean magnetic field $\overline{\mathbf{B}}$ at point $x + \xi$ by it's Taylor series[13]

$$\overline{B}_j(x + \xi, t) = \overline{B}_j(x, t) + \xi_k \frac{\partial \overline{B}_j(x, t)}{\partial x_k} + ... \tag{3.37}$$

Using this form to Eq. (3.31) results in

$$\overline{\mathcal{E}}_i(x, t) = \int\int K_{ij}(x, \xi, t, \tau) \left[\overline{B}_j(x, t) + \xi_k \frac{\partial \overline{B}_j(x, t)}{\partial x_k} + ... \right] d^3\xi \, d\tau \tag{3.38}$$

$$= a_{ij} \overline{B}_j + b_{ijk} \frac{\partial \overline{B}_j}{\partial x_k} + ... \tag{3.39}$$

Here the pseudo-tensors a_{ij} and b_{ijk}, that contain dependencies on $\overline{\mathbf{u}}$ and $\mathbf{u}'$, are

$$a_{ij} = \int\int K_{ij}(x, \xi, t, \tau) \, d^3\xi \, d\tau \tag{3.40a}$$

$$b_{ijk} = \int\int K_{ij}(x, \xi, t, \tau) \xi \, d^3\xi_k \, d\tau \tag{3.40b}$$

Typically this expansion is truncated using the second-order correlation approximation, which limits the expansion to first order of derivatives. This results in an approximation

$$\overline{\mathcal{E}}_i \approx a_{ij} \overline{B}_j + b_{ijk} \frac{\partial \overline{B}_k}{\partial x_j} \tag{3.41}$$

The kernel K is often highly localized near point (x, t) and thus the approximation should be valid to a high degree. However, the actual error depends on how well the conditions (3.35) and (3.36) hold.[6, 7]

This equation is not coordinate independent, but it can be transformed into one by writing it in terms of covariant derivative as

$$\overline{\boldsymbol{\mathcal{E}}} = \mathbf{a}\overline{\mathbf{B}} + \mathbf{b}\boldsymbol{\nabla}\overline{\mathbf{B}} \tag{3.42}$$

In this form the multiplying coefficients are tensors and as they are coordinate independent, they can be written in terms of basis tensors of second and third order.[7]

Firstly, the tensor $\mathbf{a}$ can be divided into its symmetric ($\mathbf{a}^{\mathrm{s}}$) and antisymmetric ($\mathbf{a}^{\mathrm{a}}$) parts. These two parts can now be represented by a symmetric tensor $\boldsymbol{\alpha}$ and vector $\boldsymbol{\gamma}$:

$$\begin{aligned} \mathbf{a}^{(\mathrm{s})}_{\kappa\lambda} &= \boldsymbol{\alpha}_{\kappa\lambda} \\ \mathbf{a}^{(\mathrm{a})}_{\kappa\lambda} &= \varepsilon_{\kappa\mu\lambda}\boldsymbol{\gamma}_{\mu} \end{aligned} \tag{3.43}$$

Here the indexes follow the commonly used notation where indexes of covariant tensors are marked with lower case Greek letters.

Doing the same for the $\mathbf{b}\boldsymbol{\nabla}\overline{\mathbf{B}}$ results in

$$\mathbf{b}\boldsymbol{\nabla}\overline{\mathbf{B}} = -\boldsymbol{\beta}(\boldsymbol{\nabla}\times\overline{\mathbf{B}}) - \boldsymbol{\delta}\times(\boldsymbol{\nabla}\times\overline{\mathbf{B}}) - \boldsymbol{\kappa}(\boldsymbol{\nabla}\overline{\mathbf{B}})^{(\mathrm{s})} \tag{3.44}$$

where $\boldsymbol{\beta}$ is a symmetric tensor, $\boldsymbol{\delta}$ is a vector and $\boldsymbol{\kappa}$ is a third rank tensor.

Collecting these different results together results in a famous covariant form for $\overline{\boldsymbol{\mathcal{E}}}$:[2, 7]

$$\overline{\boldsymbol{\mathcal{E}}} = \boldsymbol{\alpha}\overline{\mathbf{B}} + \boldsymbol{\gamma}\times\overline{\mathbf{B}} - \boldsymbol{\beta}(\boldsymbol{\nabla}\times\overline{\mathbf{B}}) - \boldsymbol{\delta}\times(\boldsymbol{\nabla}\times\overline{\mathbf{B}}) - \boldsymbol{\kappa}(\boldsymbol{\nabla}\overline{\mathbf{B}})^{(\mathrm{s})} \tag{3.45}$$

The coefficients $\boldsymbol{\alpha}$, $\boldsymbol{\beta}$, $\boldsymbol{\gamma}$, $\boldsymbol{\delta}$ and $\boldsymbol{\kappa}$ are called *turbulent transport coefficients* TTCs. These coefficients are widely used to characterize different physical dynamo effects.

Most famous of these terms is the $\boldsymbol{\alpha}$-term that describes the contribution of helical turbulence. This turbulence, that twists magnetic field lines in rising flux tubes and creates poloidal field from initial azimuthal fields, is crucial to dynamo action. $\boldsymbol{\beta}$ describes turbulent diffusivity. $\boldsymbol{\gamma}$-term is associated with turbulent magnetic pumping that expels magnetic fields from regions with high turbulence. $\boldsymbol{\delta}$ contributes to shear-current effect, also called Rädler effect. This effect can generate dynamo action in rotating systems with non-helical turbulence or non-rotating systems with linear shear. κ term contains contributions from additional diffusive effects.[2, 6, 7]

Calculating analytical results for the coefficients **a** and **b** from integrals (3.40a) and (3.40b) is at best very difficult and at worst borderline impossible. These calculations can be simplified by making multiple assumptions on the nature of the turbulence. Assuming isotropic and homogeneous turbulence, $\boldsymbol{\alpha}$ and $\boldsymbol{\beta}$ can be written as isotropic tensors $\boldsymbol{\alpha} = \alpha_0\delta_{\kappa\lambda}$ and $\boldsymbol{\beta} = \beta_0\delta_{\kappa\lambda}$, where $\delta_{\kappa\lambda}$ is the Kronecker delta and the magnitudes can be calculated from

$$\alpha_0 = -\frac{1}{3}\overline{\mathbf{u}\cdot(\boldsymbol{\nabla}\times\mathbf{u})}\tau_{\mathrm{corr}} \tag{3.46}$$

and

$$\beta_0 = \frac{1}{3}\overline{\mathbf{u}^2}\tau_{\mathrm{corr}} \tag{3.47}$$

A numerical method, free of specific assumptions on the nature of the turbulence, for obtaining these coefficients is described in the following chapter as an alternative to analytical methods.[7]

Chapter 4

Test-field method

Test-field method (TFM) aims to solve the turbulent transport coefficients (TTCs) from magnetohydrodynamic simulations. This chapter follows the presentation of the method given by Schrinner in 2005 in his Ph.D. dissertation.[13]

The process of applying the method goes as follows:

I. Run a full 3D MHD simulation.

II. Concurrently with the simulation solve the induction equation for the fluctuations with the velocity field obtained from step I and a series of linearly independent test fields. Use solved values of $\mathbf{B}'$ to calculate $\overline{\boldsymbol{\mathcal{E}}}$.

III. Solve TTCs from system of linear equations relating the test fields and the MEMF calculated in step II.

IV. Transform TTCs from step III to their covariant forms.

V. Post-process obtained TTCs e.g. compute their time average.

The first step is quite self-explanatory as MHD simulations are widely used to simulate the magnetic fields of the Sun (see Section 5.1 and Eq. (5.1a)-(5.1d)). From this kind of a simulation one can obtain, among other quantities of interest, $\overline{\mathbf{u}}$ and $\mathbf{u}'$ at every time step of the simulation. These fields are used by the second step of the TFM to calculate the MEMF. However, as the TFM adds a significant amount of computations to each time step of the simulation, it is usually switched on only during certain time intervals of the full simulation.

The second and third steps are the crucial steps for the method, and in the following we will present some relevant definitions and derivations to describe them in detail.

Firstly, the method relies on the assumption that the MEMF can be approximated to be a linear function of the mean magnetic field and its derivatives

$$\overline{\boldsymbol{\mathcal{E}}} = \mathbf{a}\overline{\mathbf{B}} + \mathbf{b}\boldsymbol{\nabla}\overline{\mathbf{B}} \tag{4.1}$$

As mentioned in the previous chapter, for two-scale turbulence this assumption holds.

To solve the 27 unknown coefficients of pseudo-tensors **a** and **b** one can rewrite this equation in a diagonal block matrix form as

$$\overline{\mathcal{E}}_{\kappa}^{(i)} = \left(\overline{B}_{\mathrm{T},\lambda}^{(i)},\ \frac{\partial \overline{B}_{\mathrm{T},\lambda}^{(i)}}{\partial x_{\mu}}\right) \begin{pmatrix} a_{\kappa\lambda} \\ \\ b_{\kappa\lambda\theta} \end{pmatrix} \quad , i = 1, ..., 9 \tag{4.2}$$

where the mean magnetic fields have been replaced by *test fields* $\overline{\mathbf{B}}_{\mathbf{T}}^{(i)}$ and the index i marks different test field configurations.

The test fields $\overline{\mathbf{B}}_{\mathbf{T}}^{(i)}$ do not represent the actual physical magnetic fields. Instead they act as mediators between velocity fields and the MEMF that are used to obtain the TTCs. By solving the magnetic field fluctuations and the MEMF that would occur *if the mean magnetic field was the test field under the influence of the velocity fields from the hydrodynamic simulation*, one can obtain enough known variables to solve the coefficients **a** and **b** from the set of Eqs. (4.2). Using the words of Schrinner: "$\overline{\boldsymbol{\mathcal{E}}}$ is 'measured' due to the action of the velocity field on a prescribed mean test field $\overline{\mathbf{B}}_{\mathbf{T}}$."

To obtain $\overline{\boldsymbol{\mathcal{E}}}$ one needs to solve the induction equation for the fluctuating component of the magnetic field $\mathbf{B}'$

$$\frac{\partial \mathbf{B}'}{\partial t} = \boldsymbol{\nabla} \times \overline{\mathbf{u}} \times \mathbf{B}' + \boldsymbol{\nabla} \times \mathbf{u}' \times \overline{\mathbf{B}} + \boldsymbol{\nabla} \times \mathbf{G} + \eta \nabla^2 \mathbf{B}' \tag{4.3}$$

where $\boldsymbol{G} = \mathbf{u}' \times \mathbf{B}' - \overline{\mathbf{u}' \times \mathbf{B}'}$.

Setting the mean magnetic field in to be a test field $\overline{\mathbf{B}}_\mathbf{T}$ and using the identity

$$\begin{aligned}
(\mathbf{u}\times(\overline{\mathbf{B}}_\mathbf{T}+\mathbf{B}'))' &= \mathbf{u}\times(\overline{\mathbf{B}}_\mathbf{T}+\mathbf{B}')-\overline{\mathbf{u}\times(\overline{\mathbf{B}}_\mathbf{T}+\mathbf{B}')}\\
&= ((\overline{\mathbf{u}}+\mathbf{u}')\times((\overline{\mathbf{B}}_\mathbf{T}+\mathbf{B}'))\\
&\quad -\overline{(\overline{\mathbf{u}}+\mathbf{u}')\times((\overline{\mathbf{B}}_\mathbf{T}+\mathbf{B}'))}\\
&= \overline{\mathbf{u}}\times\overline{\mathbf{B}}_\mathbf{T}+\mathbf{u}'\times\overline{\mathbf{B}}_\mathbf{T}+\overline{\mathbf{u}}\times\mathbf{B}'+\mathbf{u}'\times\mathbf{B}' \qquad (4.4)\\
&\quad -(\overline{\overline{\mathbf{u}}\times\overline{\mathbf{B}}_\mathbf{T}}+\overline{\mathbf{u}'\times\overline{\mathbf{B}}_\mathbf{T}}+\overline{\overline{\mathbf{u}}\times\mathbf{B}'}+\overline{\mathbf{u}'\times\mathbf{B}'})\\
&= \mathbf{u}'\times\overline{\mathbf{B}}_\mathbf{T}+(\mathbf{u}'\times\mathbf{B}'-\overline{\mathbf{u}'\times\mathbf{B}'})+\overline{\mathbf{u}}\times\mathbf{B}'\\
&= \mathbf{u}'\times\overline{\mathbf{B}}_\mathbf{T}+\mathbf{G}+\overline{\mathbf{u}}\times\mathbf{B}'
\end{aligned}$$

gives a *test-field induction equation*

$$\frac{\partial\mathbf{B}'}{\partial t}=\boldsymbol{\nabla}\times\left(\mathbf{u}\times(\mathbf{B}'+\overline{\mathbf{B}}_\mathbf{T})\right)'+\eta\nabla^2\overline{\mathbf{B}'} \qquad (4.5)$$

The form of the equation is similar to the classical induction equation (2.11), but there is an additional source field $\overline{\mathbf{B}}_\mathbf{T}$. Thus, with small modifications, an algorithm that integrates the equation can also solve this new equation.

To get a steady state solution for $\overline{\boldsymbol{\mathcal{E}}}$, the axisymmetric parts of $\mathbf{B}$ and $\boldsymbol{\nabla}\times\left(\mathbf{u}\times(\mathbf{B}'+\overline{\mathbf{B}}_\mathbf{T})\right)$ are set to zero at time t_0. Once $\mathbf{B}'$ reaches a steady state the value for $\overline{\boldsymbol{\mathcal{E}}}$ can be obtained by calculating the average of $\mathbf{u}'\times\mathbf{B}'$ with respect to the azimuthal direction.

For each test field of three components one obtains three values of $\overline{\boldsymbol{\mathcal{E}}}$. This means that by solving the Eq. (4.5) with 9 test fields gives enough known variables to solve the linear equation (4.2). The choice of test fields is important for this procedure. These fields need to be steady, axisymmeteric, linearly independent of each other, and their higher derivatives need to be zero. One set of test fields, for which these conditions are satisfied, is shown in Table 4.1. Columns of this table correspond to different field configurations whereas rows correspond to the components of $\overline{\mathbf{B}}_\mathbf{T}$. In each cell there is a scalar function $f = f(r,\theta,\varphi)$ that gives the magnitude of the corresponding component of $\overline{\mathbf{B}}_\mathbf{T}$ at each point (r,θ,φ).

Table 4.1: Test fields configurations

	Test-field configuration								
Field component	1	2	3	4	5	6	7	8	9
$\overline{B}_{\mathrm{T},r}$	1	0	0	r	0	0	θ	0	0
$\overline{B}_{\mathrm{T},\theta}$	0	1	0	0	r	0	0	θ	0
$\overline{B}_{\mathrm{T},\varphi}$	0	0	1	0	0	r	0	0	θ

After obtaining the MEMF the matrix equation can be solved with LR-decomposition or other methods of linear algebra. The resulting non-covariant TTCs **a** and **b** can then be transformed to covariant TTCs $\boldsymbol{\alpha}$, $\boldsymbol{\beta}$, $\boldsymbol{\gamma}$, $\boldsymbol{\delta}$ and $\boldsymbol{\kappa}$ in the same vein as in equations (3.43) and (3.44).

The end result is a set of covariant TTCs that vary in the meridional plane. The variation of coefficients over azimuthal direction is lost through the choice of the averaging operation. This approximation of axisymmetric mean-field coefficients is widely used as Sun's magnetic field is axisymmetric and features related to the mean magnetic field, such as the butterfly diagram, are obtained by taking an azimuthal average over observations.

Coefficients created by the method are time-dependent, but during post-processing they can be averaged to create time-averaged coefficients.

The presented method has been shown to be accurate and robust way of obtaining test field coefficients for multitude of different systems.[7, 8, 14]

The immediate advantage of this method compared to analytical methods is the lack of a priori assumptions. As mentioned in the previous chapter, the analytical calculation of the TTCs from integrals (3.40a) and (3.40b) is difficult and requires a priori assumptions on the nature of the turbulence. The TFM is an improvement in this regard as it can be used on arbitrary velocity fields as long as the MEMF can be represented through the linear equation (4.1).

Another practical advantage that the method provides is the possibility of utilizing it in conjunction with numerical simulations. As the numerical complexity of simulations grows

so does the difficulty of describing the occurring physical phenomena. The properties of the TTCs often contain information on the dynamos' overall structure, like the dominating dynamo effect (α^2, $\alpha\Omega$, $\alpha^2\Omega$, ...); what is the expected oscillation period or whether equatorward migration occurs. Thus a versatile tool like the TFM enables a more robust examination of complex dynamos through the TTCs.

To investigate complex systems, such as the Sun, where turbulence is driven by highly complicated convection process, a mean-field simulation code that accepts arbitrary TTCs is needed. This is the purpose of this thesis.

Chapter 5

Mean-field simulation suite

Design of the mean-field simulation suite

The mean-field simulation code was implemented in Pencil Code, which is a versatile magnetohydrodynamics simulation software maintained as a community effort and released in GitHub under open-source GPLv2 license.

Pencil Code uses high-order finite-difference methods to solve compressible magnetohydrodynamic equations. The name of the simulation suite comes from its utilization of ”pencils”, x-dimension sized vectors that are used to store temporary variables needed during the time integration. This is done in order to reduce processor cache misses during the time integration phase as relevant quantities are stored into memory in vectors with the length of the x dimension. In each timestep and each point in the y- and z-directions the code calculates these pencils and after they are calculated it uses them to calculate a new state of the system. When calculating spatial derivatives, Pencil Code uses sixth-order finite-difference derivatives.[15]

Time stepping is done with a three-step Runge-Kutta method. To minimize the amount of memory required for variables Pencil Code uses a 2N-scheme, where the state of the system is stored in an array f which is then used to calculate a changed state df using the aforementioned pencils. New state of f is then calculated from df using the Runge-Kutta time-integration scheme.[15, 16]

Parallelization for the code is done with MPI and there exists a module system that can be used to extend the code with additional physics.[15]

The magnetohydrodynamic equations that Pencil Code is capable of solving consist of continuity equation, compressible Navier-Stokes equation, induction equation and entropy equation. These equations can be written as

$$\frac{D\ln\rho}{Dt} = -\boldsymbol{\nabla}\cdot\mathbf{u} \tag{5.1a}$$

$$\frac{D\mathbf{u}}{Dt} = -c_s^2\boldsymbol{\nabla}\left(\frac{s}{c_p}+\ln\rho\right) - \boldsymbol{\nabla}\Phi_{\text{grav}} + \frac{\mathbf{j}\times\mathbf{B}}{\rho} + \nu\left(\nabla^2\mathbf{u} + \frac{1}{3}\boldsymbol{\nabla}\boldsymbol{\nabla}\cdot\mathbf{u} + 2\mathbf{S}\cdot\boldsymbol{\nabla}\ln\rho\right) + \zeta\left(\boldsymbol{\nabla}\boldsymbol{\nabla}\cdot\mathbf{u}\right) \tag{5.1b}$$

$$\frac{\partial\mathbf{A}}{\partial t} = \mathbf{u}\times\mathbf{B} - \eta\mu_0\mathbf{j} \tag{5.1c}$$

$$\rho T\frac{Ds}{Dt} = \mathcal{H} - \mathcal{C} + \boldsymbol{\nabla}\cdot(K\boldsymbol{\nabla}T) + \eta\mu_0\mathbf{j}^2 + 2\rho\nu\mathbf{S}\otimes\mathbf{S} + \zeta\rho(\boldsymbol{\nabla}\cdot\mathbf{u})^2 \tag{5.1d}$$

Here ρ is the matter density, $\mathbf{u}$ is velocity, c_s is the speed of sound in the matter, s is entropy, c_p is the specific heat at constant pressure, Φ_{grav} is the gravity potential, $\mathbf{j}$ is the current density, $\mathbf{B}$ is the magnetic field, ν is kinematic viscosity, ζ is bulk viscosity, η is magnetic diffusivity, $\mathbf{S}$ is rate-of-shear tensor, T is the temperature, K is thermal conductivity, $\mathcal{H}$ and $\mathcal{C}$ are explicit heating and cooling terms for boundary conditions, and $\otimes$ denotes the tensor contraction operation.[15]

These equations are valid when the system in question satisfies magnetohydrodynamic approximation. For this approximation to be valid the gas should behave like a continuous fluid where the size of the system is much larger than any distance of interest, which in turn is much larger than distances between particles. Similarly the mean interaction time between particles should be much shorter than the simulated timescale. This approximation holds for all simulations done for this work.[17]

The modular way in which Pencil Code has been created allows users to modify these equations or even refrain from utilizing them. For non-generic use cases there is also a system for special modules that can be used to modify existing equations with minimal changes required to the existing code. There also exists a versatile Python interface that can be used to access simulation results.[15]

An important module for this work is an existing implementation of the TFM that can be used to calculate TTCs. This module has been validated with known, analytically solvable, test cases and it has been previously used to analyze TTCs in simulated dynamo systems.[8, 14]

For the purpose of this work the three used module combinations are

(a) Induction equation module and a special module for mean magnetic field:

Used to simulate mean magnetic fields.

(b) Hydrodynamics modules and a special module for TFM:
Used to generate TTCs.

(c) All magnetohydrodynamic modules:
Used to obtain the full 3D magnetic field solution for reference.

The implementation was done as three separate programs:

(a) Python script that can be used to create TTCs from different analytical theories.

(b) Python script that can be used to create TTCs from the output of the TFM.

(c) A special module in Pencil Code that can be used to solve mean-field induction equation (Eq. (5.10)) with arbitrary combination of TTCs ($\boldsymbol{\alpha}, \boldsymbol{\beta}, \boldsymbol{\gamma}, \boldsymbol{\delta}, \boldsymbol{\kappa}$) and the mean velocity field ($\overline{\mathbf{u}}$).

This choice was motivated by many factors.

Firstly, the TFM and mean-field simulations have different computational requirements. While the TTCs are usually calculated by tens of MPI workers in a three-dimensional grid, solving the mean-field induction equation requires a two-dimensional grid with few MPI workers. As the splitting of the simulation grid depends on the number MPI workers, the TTCs created with the TFM need to be split in a new fashion for the mean-field simulation.

Secondly, the data format for the TTCs should be transferable across different systems. Pencil Code has two output strategies: collective and distributed. With collective strategy the first MPI worker writes all outputs to its data folder. This scales badly across multiprocessor simulations and is typically not used for large-scale simulations. With distributed strategy each MPI worker writes output to their own folder. The advantage of this method is a large speedup in I/O operations, but with this method the handling of the data becomes harder as it is split. Both methods result in machine-dependent output. This means that in a situation, where the TFM is run on a larger system and the data is transferred to a smaller system for the mean-field simulation, one cannot assume that the data structuring stays the same. Especially when changing from three-dimensional grid to a two-dimensional grid one needs to adapt the TTCs.

To address these problems Hierarchial Data Format (HDF) revision 5 (HDF5) was chosen as a storage format for the TTCs. HDF5 is hierarchical, portable and parallelizable data

format that is widely used by different scientific applications. Using HDF5 in data I/O has been previously tried in Pencil Code, but the module responsible for it was never completed. Thus completing and testing a parallel implementation of HDF5 I/O was an interesting technical goal of this work.

Thirdly, the preprocessing code should be able to create a set of desired TTCs from a chosen analytical theory or from an existing test-field simulation. Due to its existing libraries, these task were easiest to implement in Python. Pencil Code has a Python API that was used to provide coordinate grids and turbulent-transport coefficients from the test-field simulations to the pre-processing code. In addition to this API, scientific libraries NumPy and SciPy, that contain advanced numerical routines, and h5py, a HDF5 interface library, were used to create analytical coefficients and write them to HDF5 files respectively.

The workflows for the two different use cases, test-field based coefficients and analytical coefficients, are shown in Figure (5.1).

For analytical TTCs, the mean-field simulation code needs to be initialized so that the simulation grid can be used for the creation of the coefficients. This coordinate grid is then loaded by a *coefficient creation factory*. The factory will create TTCs based on these parameters:

- Coefficient name, that describes which coefficient would be created (e.g. ”alpha”, ”beta”).
- Unique dataset name, that is used to distinguish different coefficients (e.g. ”isotropic”, ”Steenbeck-Krause-1969-model1”).
- An multidimensional array of floating point numbers or functions, that is used to obtain values for the coefficient’s components. The indices of this array correspond to the indices of the coefficient to be created (e.g. $\boldsymbol{\alpha}$ would require a 3 times 3 array). The functions can use coordinates of the simulation grid and the time coordinate to obtain the value of the component at each point z, y, x, t.
- A list of time values, for which the coefficients will be evaluated. Time dependent coefficients are not used in this work, but the possibility of creating them was implemented.

Using this structure and Python’s lambda-functions, coefficients for multiple different analytical models can be created easily. Example coefficient parameters, that generate $\boldsymbol{\alpha}$ for model described in section 6.4, are given in program example (5.1).

```
{
    'coefficient': 'alpha',
    'dataset': 'Steenbeck-Krause-1969-model1',
    'values': [
              [0, 0, 0],
              [0, 0, 0],
              [0, 0, lambda z, y, x, t: 0.5*(1+scipy.special.erf((x-0.9)/0.075))*numpy.cos(y)],
              ],
    'tvals': [1]
},
```

Program example 5.1: Syntax of the coefficient creation factory

This particular example produces an $\boldsymbol{\alpha}$-coefficient that is zero with the exception of

$$\alpha_{\varphi\varphi} = \frac{1}{2}\left\{1 + \Phi\left(\frac{r - r_2}{d_2}\right)\right\}\cos\theta \quad , \tag{5.2}$$

where $r_2 = 0.9$ and $d_2 = 0.075$.

When creating TTCs from the output of the test-field model, a different Python script is used. This script transforms the pseudotensors **a** and **b**, obtained from the TFM, to covariant forms $\boldsymbol{\alpha}$, $\boldsymbol{\beta}$, $\boldsymbol{\gamma}$, $\boldsymbol{\delta}$ and $\boldsymbol{\kappa}$. In addition the mean velocity field $\overline{\mathbf{u}}$ is stored in a group called ”utensor”.

At this point the datasets can be smoothed in both time and space and upscaled (downscaled) to match a more dense (sparse) grid size for the mean-field simulation. When pre-processing coefficients for the model in section 6.6, arithmetic mean was used to get time averaged coefficients, but no spatial smoothing or scaling was done.

For both workflows the TTCs are stored in a single file and organized in a hierarchical data structure. This data structure is visualized in Figure 5.2. HDF5 allows grouping of different datasets and this is done for grid vectors (”/grid”) and TTCs (”/emftensors”). Every TTC is also a grouping. The mean velocity field is added as a separate field (”utensor”) as the mean-field solver does not calculate hydrodynamics. These groupings enable the storage of different models in the same input file. For example, the dataset created by code (5.1) is stored in ”/emftensor/alpha/Steenbeck-Krause-1969-model1”.

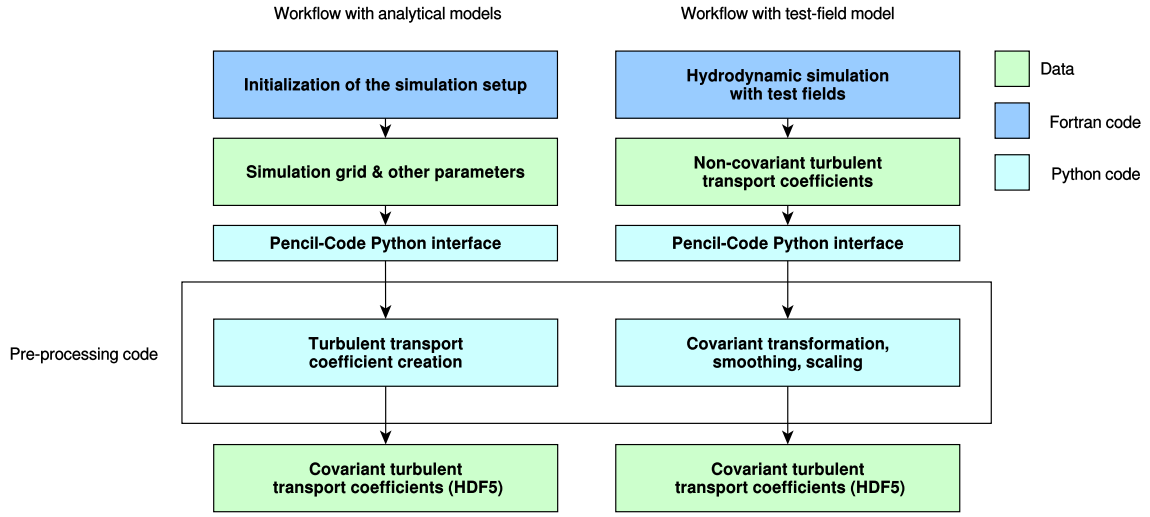

Figure 5.1: The pre-processing steps for two workflows

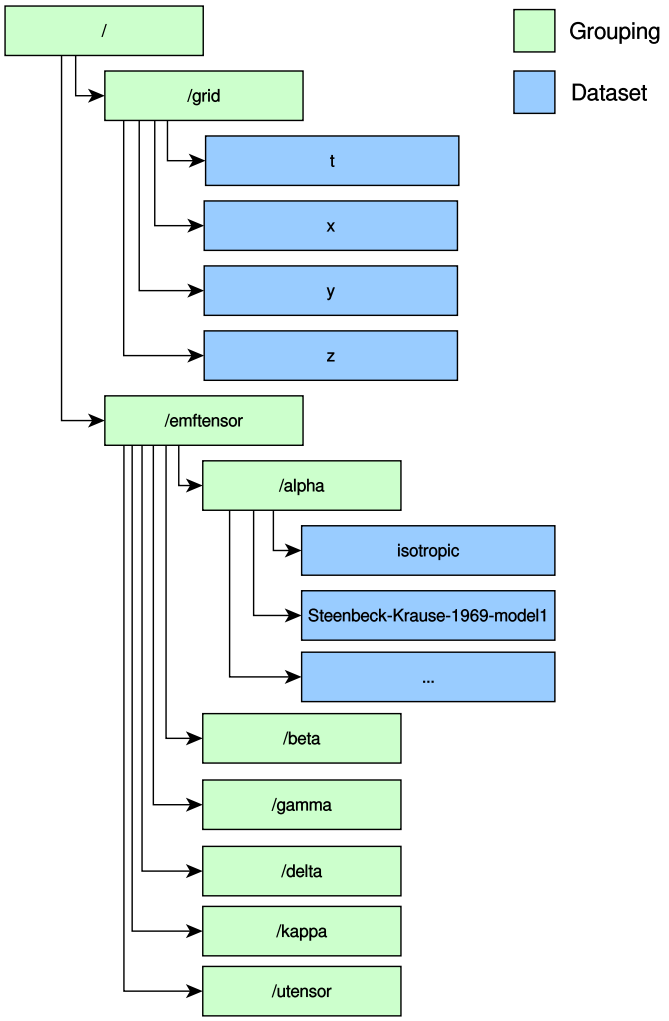

Figure 5.2: Chosen HDF 5 data format

Mean-field solver implementation

The new module was written as a special module that uses the existing magnetic module to solve the mean-field induction equation. The magnetic module obtains the magnetic field from the magnetic vector potential, which is calculated using Eq. (5.1c).

The mean-field induction equation (Eq. (3.7))

$$\frac{\partial \overline{\mathbf{B}}}{\partial t} = \boldsymbol{\nabla} \times \left(\overline{\mathbf{u}} \times \overline{\mathbf{B}} + \overline{\boldsymbol{\mathcal{E}}} - \eta \mu_0 \overline{\mathbf{J}} \right) \tag{5.3}$$

can be written in terms of mean-field vector potential by starting from the equation relating the magnetic field and the vector potential

$$\mathbf{B} = \boldsymbol{\nabla} \times \mathbf{A} \tag{5.4}$$

Splitting it into mean and fluctuating parts results in

$$\overline{\mathbf{B}} + \mathbf{B}' = \boldsymbol{\nabla} \times \overline{\mathbf{A}} + \boldsymbol{\nabla} \times \mathbf{A}' \tag{5.5}$$

and applying the averaging operator to this equation gives

$$\overline{\mathbf{B}} = \boldsymbol{\nabla} \times \overline{\mathbf{A}} \tag{5.6}$$

Inserting this to the mean-field induction equation gives

$$\boldsymbol{\nabla} \times \frac{\partial \overline{\mathbf{A}}}{\partial t} = \boldsymbol{\nabla} \times \left(\overline{\mathbf{u}} \times \overline{\mathbf{B}} + \overline{\boldsymbol{\mathcal{E}}} - \eta \mu_0 \overline{\mathbf{J}} \right) \tag{5.7}$$

Moving everything to the left side and taking curl as a common operator results in

$$\boldsymbol{\nabla} \times \left(\frac{\partial \overline{\mathbf{A}}}{\partial t} - \overline{\mathbf{u}} \times \overline{\mathbf{B}} - \overline{\boldsymbol{\mathcal{E}}} + \eta \mu_0 \overline{\mathbf{J}} \right) = 0 \tag{5.8}$$

Uncurling this equation gives

$$\frac{\partial \overline{\mathbf{A}}}{\partial t} - \overline{\mathbf{u}} \times \overline{\mathbf{B}} - \overline{\boldsymbol{\mathcal{E}}} + \eta \mu_0 \overline{\mathbf{J}} = \boldsymbol{\nabla} \varphi \tag{5.9}$$

where φ is the electric potential. By adopting the Weyl gauge, that is defined by $\varphi = 0$, this term can be omitted.

Reorganizing this equation results in a mean-field induction equation written in terms of the vector potential

$$\frac{\partial \overline{\mathbf{A}}}{\partial t} = \overline{\mathbf{u}} \times \overline{\mathbf{B}} + \overline{\boldsymbol{\mathcal{E}}} - \eta \mu_0 \overline{\mathbf{J}} \tag{5.10}$$

From this form of the obtained induction equation, when compared with the standard equation (Eq. (5.1c)) that the Pencil Code solves, we see that in the special module we need to compute the value of $\overline{\boldsymbol{\mathcal{E}}}$ and $\overline{\mathbf{u}} \times \overline{\mathbf{B}}$ and add them to the right side of the equation (5.1c).

To enable different mean-field models, the covariant forms of TTCs presented in Equation (3.45) are used to define the initial parameters. The calculation of $\overline{\boldsymbol{\mathcal{E}}}_{\text{total}}$ is done in parts by writing

$$\begin{aligned}
\overline{\boldsymbol{\mathcal{E}}}_{\text{total}} &= \overline{\mathbf{u}} \times \overline{\mathbf{B}} + \boldsymbol{\alpha}\overline{\mathbf{B}} + \boldsymbol{\gamma} \times \overline{\mathbf{B}} \\
&\quad -\boldsymbol{\beta}(\boldsymbol{\nabla} \times \overline{\mathbf{B}}) - \boldsymbol{\delta} \times (\boldsymbol{\nabla} \times \overline{\mathbf{B}}) - \boldsymbol{\kappa}(\boldsymbol{\nabla}\overline{\mathbf{B}})^{(\mathrm{s})} \\
&= \overline{\mathbf{u}} \times \overline{\mathbf{B}} + \boldsymbol{\alpha}\overline{\mathbf{B}} + \boldsymbol{\gamma} \times \overline{\mathbf{B}} - \boldsymbol{\beta}\overline{\mathbf{J}} - \boldsymbol{\delta} \times \overline{\mathbf{J}} - \boldsymbol{\kappa}(\boldsymbol{\nabla}\overline{\mathbf{B}})^{(\mathrm{s})} \\
&= \overline{\boldsymbol{\mathcal{E}}}_{\mathrm{u}} + \overline{\boldsymbol{\mathcal{E}}}_{\alpha} + \overline{\boldsymbol{\mathcal{E}}}_{\gamma} - \overline{\boldsymbol{\mathcal{E}}}_{\beta} - \overline{\boldsymbol{\mathcal{E}}}_{\delta} - \overline{\boldsymbol{\mathcal{E}}}_{\kappa}
\end{aligned} \tag{5.11}$$

The mathematical operations required to calculate these terms are already present in Pencil Code as subroutines. An often used convention of choosing positive signs to advective terms and negative signs for diffusive terms is chosen throughout the code.

The TTCs are loaded from input data file to variables and their amplitudes are scaled during runtime by a user-defined factor. The additional scaling factor made the search of eigenvalues in simulations with analytical solutions easier, as recreating coefficients was not required to rescale them.

At each time step the requested x-sized pencil of the coefficient is taken from the variable array. Contribution of each term to the MEMF is calculated based on user request, so no additional calculation is done in a case when terms are not needed. To minimize rounding errors, each term was added individually to a common pencil that is then added as a contribution to the equation solving the normal induction equation.

An additional extension was created to make disabling individual components of the TTCs possible. This was not used in the models presented here, but it was designed and implemented for future applications. During pencil loading the possibility of using time dependent transport coefficients was taken into account by creating a function callback that can interpolate the input coefficients based on the current time. The coefficients used in the models presented here were, however, time averages, and therefore time independent. Using time-independent tensors was deemed adequate for the purpose of testing the mean-field simulation suite and the TFM.

Chapter 6

Mean-field simulations

The new mean-field simulation suite was used to model different mean-field configurations. These configurations were divided into two main categories:

I. Analytically solvable systems with known TTCs. These simulations were used to validate the correctness of the mean-field simulation suite.

II. A mean-field simulation that uses TTCs obtained with the TFM. This simulation is used to validate the test-field module (TFMod).

Simulations of type I include:

1. System with constant isotropic α-effect. Comparison was done to a book by Krause and Rädler (1980).[6]

2. System with constant isotropic β-effect. Comparison was done to Pencil Code's implementation of the same effect.

3. System with α-effect and differential rotation. Comparison was done to article by Steenbeck and Krause (1969).[18, 19]

4. System with α-effect, differential rotation and spatially varying isotropic β-effect. Comparison was done to article by Jouve et al. (2008).[20]

Simulation of type II is an α^2-dynamo driven by helically forced turbulence. This model is similar to a model run and investigated by Mitra et al. (2010). The TTCs used in this

simulation were obtained with the TFM. The magnetic fields obtained from this simulation were then compared to magnetic fields obtained from a DNS. Results of this simulation were published in a paper by Warnecke et al..[8, 12]

Simulation parameters and boundary conditions

For all models the fields were considered to be azimuthal averages and thus the simulations could be done in a two dimensional wedges ranging from $r \in [r_0, r_1]$ in the radial direction and $\theta \in [\theta_0, \pi - \theta_0]$ in the colatitudinal direction. The constants r_0, r_1 and θ_0 were chosen to match the values given in articles.

During the simulations this wedge was divided into a $n \times m$ grid. Grid size was 64x128 for the validation models and 128x256 for the test-field model.

All simulations were run in Aalto University's Triton cluster and parallelized with OpenMPI. Validation models were done with 4 processors while the test-field model used 8 processors. The test-field model and corresponding magnetohydrodynamic simulation were done by Dr. Jörn Warnecke and they were run in CSC's Taito-cluster.

For all simulations the inner boundary $r = r_0$ was assumed to behave as a perfect conductor. This widely used boundary condition is satisfied when[8, 20, 21, 22]

(a) There is no radial magnetic fields across the boundary: $B_r = 0$

(b) There is no transverse current on the inner boundary: $j_\theta = j_\varphi = 0$

At the outer boundary $r = r_1$ the magnetic field was assumed to and normal to the boundary. This is another widely used boundary condition that can be summed up with equation[8, 20, 21]

$$B_\theta = B_\varphi = 0 \tag{6.1}$$

Two different boundary conditions were used for the θ boundary at $\theta = \theta_0$ and $\theta = \pi - \theta_0$. All validation simulations used regularity condition (SAA condition), for which

$$\frac{\partial A_r}{\partial \theta} = A_\theta = A_\varphi = 0 \tag{6.2}$$

on the boundary. Here S and A stand for symmetry or antisymmetry of the corresponding vector potential component at the border.

For the test-field simulation this SAA boundary conditions results in unwanted non-oscillatory behavior. Similar results were also seen in mean-field simulations by Cole et al. and thus perfect conductor condition was used.[22]

This perfect conductor condition (ASA condition) is satisfied when

$$A_r = \frac{\partial A_\theta}{\partial \theta} = A_\varphi = 0 \tag{6.3}$$

Isotropic α-effect

Description

The simplest case to consider is a sphere of radius R that consists of electrically conducting material sitting in a vacuum. Now due to some unknown process there exists steady, isotropic and non-mirror-symmetric turbulance within it. There does not exist any mean flow of material and the scale separation holds. Furthermore, the turbulent diffusivity of the system is isotropic. This kind of system is fully determined by α- and β-effects and a steady state solution, where α-effect induces the magnetic fields which the β-effect then diffuses, can be found.[6]

Written in the notation of the previous chapters, the $\boldsymbol{\alpha}$-tensor is $\alpha_{ij} = \alpha_0 \delta_{ij}$, $\boldsymbol{\beta}$ is $\beta_{ij} = \beta_0 \mu_0 \delta_{ij}$ and the mean velocity field $\overline{\mathbf{u}} = 0$. Substituting these terms to equation (5.10) reduces it into a linear differential equation

$$\frac{\partial \overline{\mathbf{A}}}{\partial t} = -\beta_0 \mu_0 \overline{\mathbf{J}} + \alpha_0 \overline{\mathbf{B}} \tag{6.4}$$

By using Ampere's law this can be written as

$$\frac{\partial \overline{\mathbf{A}}}{\partial t} = -\beta_0 \boldsymbol{\nabla}^2 \overline{\mathbf{A}} + \alpha_0 \boldsymbol{\nabla} \times \overline{\mathbf{A}} \tag{6.5}$$

In steady case this equation reduces to

$$\alpha_0 \boldsymbol{\nabla} \times \overline{\mathbf{A}} - \beta_0 \boldsymbol{\nabla}^2 \overline{\mathbf{A}} = 0 \tag{6.6}$$

Solutions for this equation can be found by using toroidal-poloidal-decomposition In toroidal-poloidal-decomposition the field is separated to toroidal and poloidal fields

generated from two scalar functions S and T.

$$\begin{aligned} \overline{\mathbf{B}} &= \overline{\mathbf{B}}_t + \overline{\mathbf{B}}_p \\ \overline{\mathbf{B}}_p &= \boldsymbol{\nabla} \times \overline{\mathbf{A}}_t \\ \overline{\mathbf{B}}_t &= -r \times \boldsymbol{\nabla} T \\ \overline{\mathbf{A}}_t &= -r \times \boldsymbol{\nabla} S \end{aligned} \tag{6.7}$$

These functions can in turn be written in terms of spherical harmonics Y_n^m:

$$\begin{aligned} T(\mathbf{r},t) &= \sum_{n,m} T_n^m(r,t) Y_n^m(\theta,\varphi) \\ S(\mathbf{r},t) &= R \sum_{n,m} S_n^m(r,t) Y_n^m(\theta,\varphi) \end{aligned} \tag{6.8}$$

Here R is the radius of the sphere.

These solutions are characterized by a dimensionless dynamo numbers $C_\alpha^{nm} = \alpha R/\eta_\mathrm{T}$ for corresponding numbers n,m. For these dynamo numbers the resulting solutions are steady state solutions with the field configurations determined by the eigenfunctions. The eigenstates corresponding to n and l are degenerate with respect to m, so the state $m = 1$ is the first state to be exited. The first eigenvalue for this system is $C_\alpha^{11} = 4.4934$ and with $m = 0$ it represents an axisymmetric magnetic field with dipole symmetry.

In non-steady case the equation (6.6), assuming that the solution is an exponential one, is solved by using functions

$$\begin{aligned} T_n^m &= T_{nl}^m \exp\{\lambda_{nl} t\} \\ S_n^m &= S_{nl}^m \exp\{\lambda_{nl} t\} \end{aligned} \tag{6.9}$$

where λ_{nl} is a growth rate that depends on a dynamo number C and T_{nl}^m and S_{nl}^m are spatially varying scalar functions that can be written in terms of Bessel functions. For each value of C and n there exists an infinite number of values for λ_{nl}, but due to the fact that modes with lowest values of n and l are exited first, the sign of λ_{11} determines the behavior of the system as a whole. Thus, given a value of C, if $\lambda_{11} > 0$ the solutions are exponentially growing and if $\lambda_{11} < 0$ they are exponentially decaying. The first value of C, for which the solutions are neither growing nor decaying, matches the first eigenvalue

of the static system $C_\alpha^{11} = 4.4934$. This eigenvalue is called *the critical dynamo number* or *the marginal value of* C, afterwards written as C_α^* [6, 22, 23]

Main measured quantities of the simulation of this model are the magnitude of the critical dynamo number C_α^*, the evolutionary behavior of the system and comparison of the analytical magnetic field profiles with the simulated ones.

Simulation domains were set at $r \in [0.1, 1.0]$ and $\theta \in [0, \pi]$. A region near the center of the sphere had to be omitted as higher density of the simulation grid points would have increased the simulation time as the characteristic time step of the system depends on the grid density.

Results

The evolution of the rms value of magnetic field $\overline{B}_{\text{rms}} = \sqrt{\left\langle \overline{\mathbf{B}}^2 \right\rangle}$ was found to depend on the value of C_α as expected. Figure (6.1a) shows how $\ln \overline{B}_{\text{rms}}$ as a function of t for values of C_α close to the C_α^*. In simulations where $C_\alpha < C_\alpha^*$ the fields were exponentially decaying and beyond the critical dynamo number $C_\alpha > C_\alpha^*$ exponential growth was encountered.

As $\lambda \propto \frac{\ln \overline{B}_{\text{rms}}}{t}$, fitting an line to $\ln \overline{B}_{\text{rms}}$ provides the value of λ. This fitting was done only to the end of the dataset where the dynamo had already reached its eigenstate. The values of λ have been plotted against the value of C_α in Figure 6.1b.

For $C_\alpha < C_\alpha^*$ the value of λ was found to be negative and beyond the critical dynamo number $C_\alpha^* \approx 4.551$, the value of λ keeps growing linearly. There exists a difference of a few percent in between the observed and expected eigenvalues. This is most likely due to the missing inner region in the simulation setup. Nevertheless the match can be considered good.

Figures 6.2a,6.3a and 6.4a show the components of the mean magnetic field generated by $C_\alpha = 5$ while figures 6.2b,6.3b and 6.4b show the first eigenstate of the analytical solutions ($n = 1, l = 1, m = 0$). A simulation in the growing regime was chosen as it obtains the eigenstate faster than simulations near the marginal value. The eigenmodes match well together, but the missing inner region causes boundary effects. The toroidal field is especially affected by this.

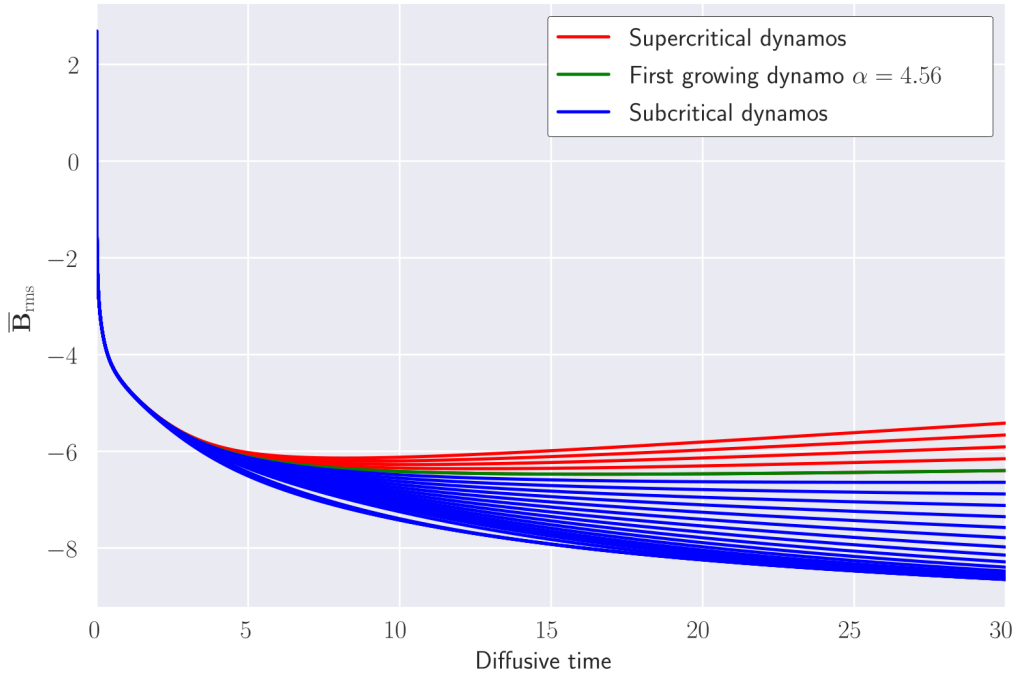

(a) Evolution of $\overline{B}_{\mathrm{rms}}$ for different values of C_α

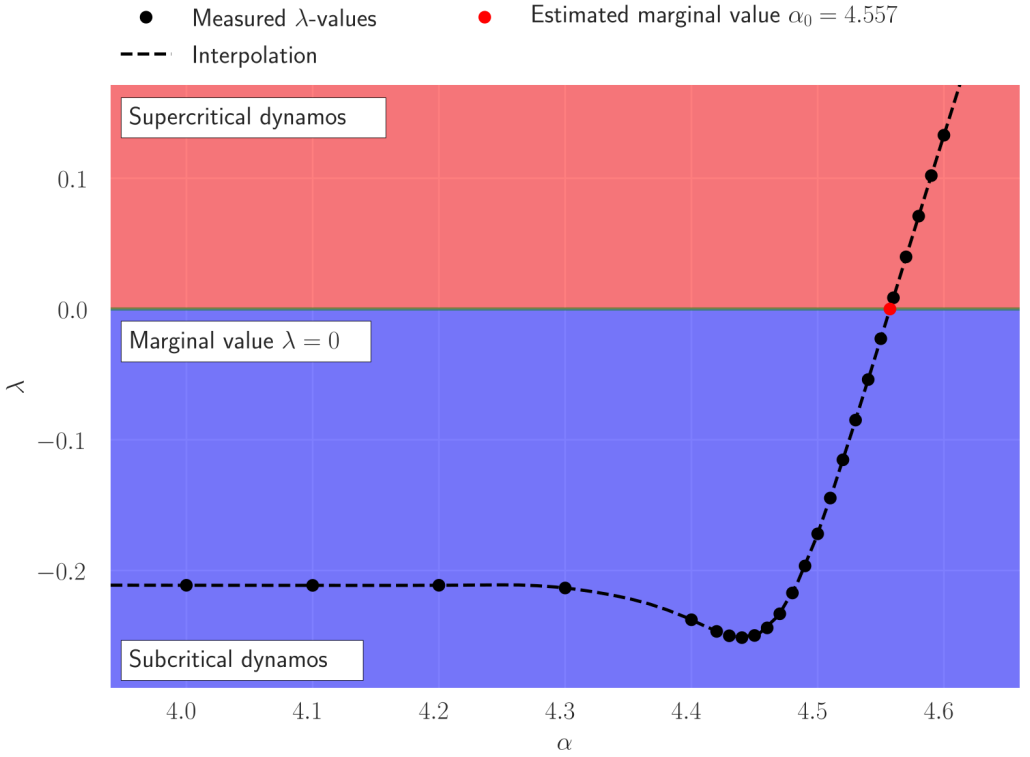

(b) Dependency of the growth rate λ on C_α

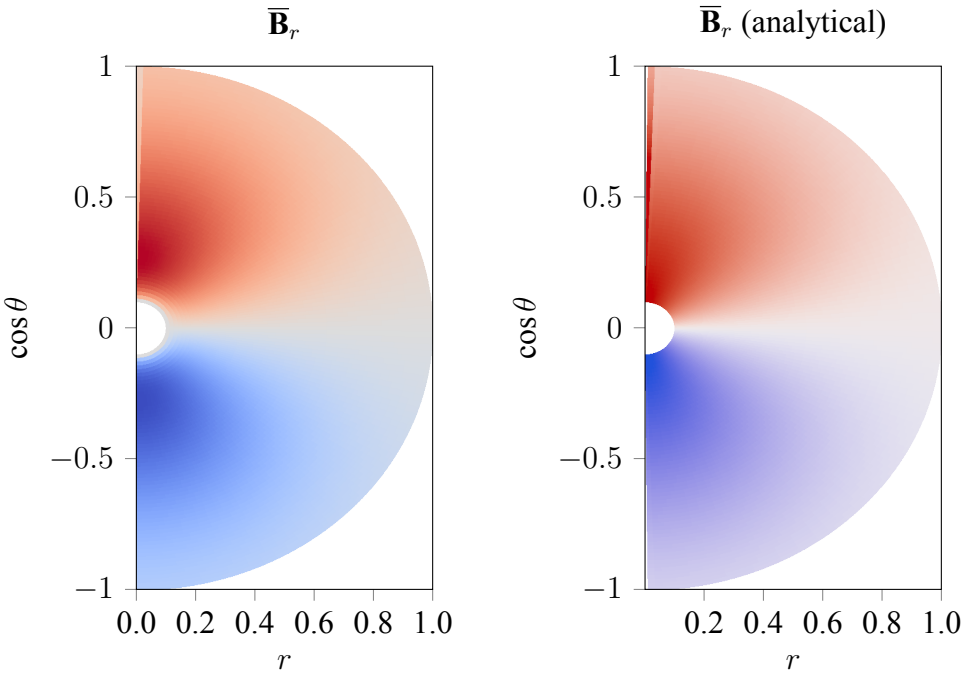

(a) Simulated $\overline{\mathbf{B}}_r$-field

(b) Analytical eigenstate

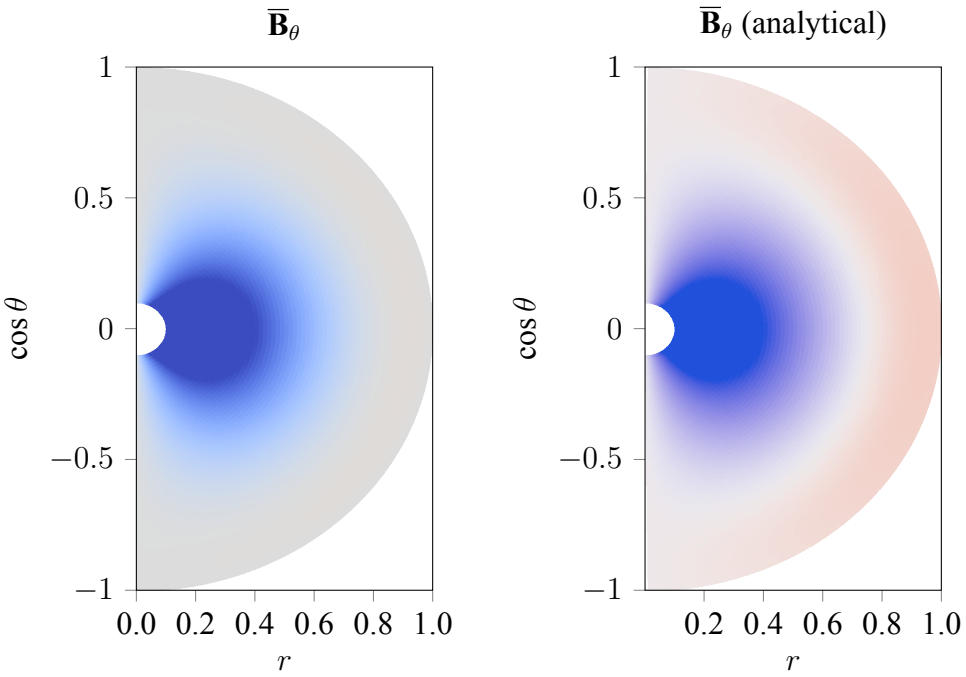

(a) Simulated $\overline{\mathbf{B}}_\theta$-field

(b) Analytical eigenstate

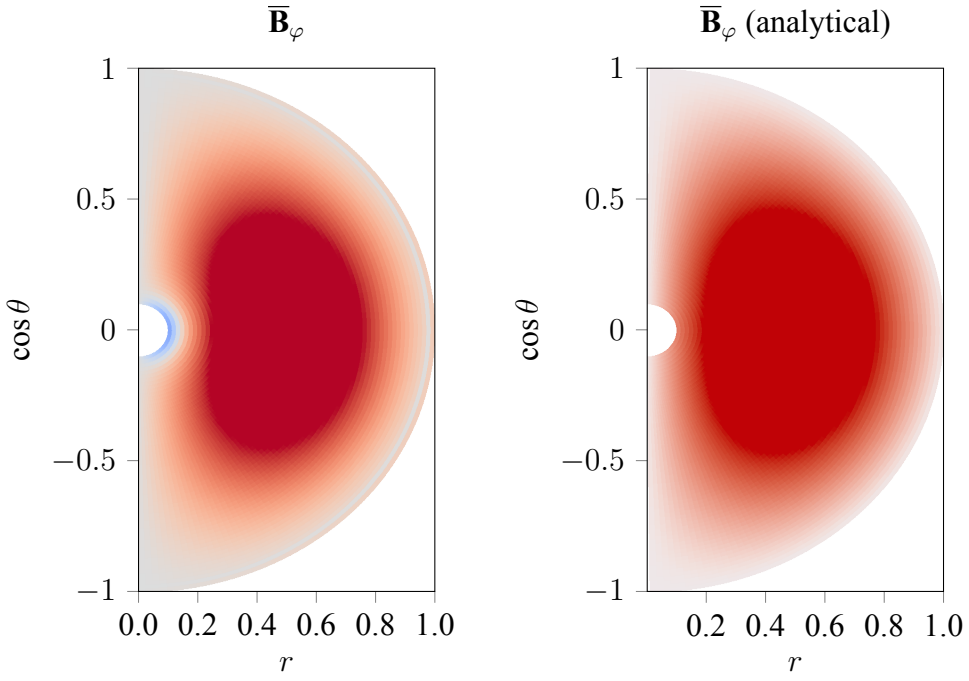

(a) Simulated $\overline{\mathbf{B}}_\varphi$-field

(b) Analytical eigenstate

Isotropic β-effect

Description

The β-tensor is associated with turbulent diffusivity, which is diffusion through the random motions of the turbulent matter. Due to the powerful turbulence in the solar convection zone the turbulent diffusivity can often dominate over the conventional molecular resistivity caused by ion-ion collisions. This makes taking this effect into account important for simulations of the convection zone.[2]

In real stars the turbulence is anisotropic, but in order to test the simulation code the used turbulence was considered to be isotropic. This allows for the $\boldsymbol{\beta}$-tensor to be written in the form $\beta_{ij} = \eta_T \mu_0 \delta_{ij}$, that was obtained in chapter 3.4. Setting $\overline{\mathbf{u}} = 0$ and $\overline{\boldsymbol{\mathcal{E}}} = -\boldsymbol{\beta} \cdot (\boldsymbol{\nabla} \times \overline{\mathbf{B}})$

to Equation (5.10) results in

$$\begin{aligned} \frac{\partial \overline{\mathbf{A}}}{\partial t} &= -\eta\mu_0\overline{\mathbf{J}} - \boldsymbol{\beta}\cdot(\boldsymbol{\nabla}\times\overline{\mathbf{B}}) \\ &= -\eta\mu_0\overline{\mathbf{J}} - \eta_T\mu_0\overline{\mathbf{J}} \\ &= -(\eta+\eta_T)\mu_0\overline{\mathbf{J}} \end{aligned} \tag{6.10}$$

Here Ampere's law is assumed to hold.

From this equation it is apparent that running different simulations with varying values of η and η_T should give same results, as long as their sum $\eta + \eta_T$ remains unchanged.

By running the simulation with various combinations of $\eta_T \in [0,1]$ and $\eta = 1 - \eta_T$ on a randomly seeded initial condition, the implementation of the turbulent diffusivity in the MFMod can be tested against the existing magnetic module.

Results

In order to measure the possible difference between the implementations, a pointwise comparison was made to a magnetic field $\overline{\mathbf{B}}_0(t,\mathbf{x})$ generated with the already existing magnetic module. The rms difference of fields divided by the rms value of the reference field was calculated at each coordinate point across snapshots taken at multiple times:

$$R_{\eta_T}(t,\mathbf{x}) = \frac{\sqrt{\sum_{i=0}^{2}\left[\overline{B}_{\eta_T,i}(t,\mathbf{x}) - \overline{B}_{0,i}(t,\mathbf{x})\right]^2}}{\overline{B}_{0,\mathrm{rms}}(t,\mathbf{x})} \tag{6.11}$$

The maximum and mean values of $R_{\eta_T}(t,\mathbf{x})$ were calculated for each value of η_T and the results obtained are shown in Table (6.1). As the simulation was done in double precision with 15-17 significant digits, an overall result of $\langle R_{\eta_T}\rangle = \mathcal{O}(10^{-12})$ and $\max(R_{\eta_T}) = \mathcal{O}(10^{-8})$ can be considered very good.

Table 6.1: Difference between two implementations of isotropic diffusivity

η_T	η	$\langle R_{\eta_T} \rangle$	$\max(R_{\eta_T})$
0.00	1.00	0	0
0.10	0.90	1.4×10^{-12}	1.8×10^{-8}
0.20	0.80	1.3×10^{-12}	2.3×10^{-8}
0.30	0.70	1.4×10^{-12}	1.1×10^{-8}
0.40	0.60	1.3×10^{-12}	2.6×10^{-8}
0.50	0.50	1.4×10^{-12}	2.3×10^{-8}
0.60	0.40	1.4×10^{-12}	1.1×10^{-8}
0.70	0.30	1.4×10^{-12}	1.0×10^{-8}
0.80	0.20	1.3×10^{-12}	1.3×10^{-8}
0.90	0.10	1.4×10^{-12}	2.1×10^{-8}
1.00	0.00	1.3×10^{-12}	2.3×10^{-8}

Steenbeck-Krause-dynamo

Description

In the first part of a two-part article ”On the dynamo theory of stellar and planetary magnetic fields fields” (1969) Steenbeck and Krause[18] calculated analytical and numerical solutions for solar dynamo models. The article in question was translated to English by Roberts and Stix in 1971[19] and the following chapter will be based on that translation. The mean-field model presented here is based on model 1 of that article that describes isotropic $\boldsymbol{\alpha}$-effect in the presence of differential rotation with varying complexities to make the model more realistic.

In their model they consider a star of radius R with solidly rotating core contained within a more slowly rotating convection zone with a relatively slowly varying magnetic field $\overline{\mathbf{B}}$.

For different models the paper describes various different rotation profiles defined by

$$\Omega(r, \theta) = \Omega_0 \left(\widetilde{\Omega}_0(r) + \widetilde{\Omega}_1(r) P_2(\cos\theta) \right) \tag{6.12}$$

where Ω_0 is a scalar magnitude factor, $P_2(\cos\theta)$ is the second Legendre polynomial and

functions $\widetilde{\Omega}_0(r)$ and $\widetilde{\Omega}_1(r)$ define the radial profile of the rotation.

However, tests were done only against the simplest model 1, for which $\widetilde{\Omega}_1(r) = 0$ and

$$\widetilde{\Omega}_0(r) = \frac{1}{2}\left\{1 - \Phi\left(\frac{r - r_1}{d_1}\right)\right\} \tag{6.13}$$

resulting in a rotation profile

$$\Omega(r, \theta) = \frac{\Omega_0}{2}\left\{1 - \Phi\left(\frac{r - r_1}{d_1}\right)\right\} \tag{6.14}$$

Here Φ is the error function and constants r_1 and d_1 determine the inner radius and the width of the transition area of the Ω profile respectively. From Equation (6.14) it is apparent that at the bottom of the convection zone the rotation rate matches core's solid rotation $\Omega(r_1) = \Omega_0$ and at the top of it reaches the value $\Omega(R) = 0$.

For the MFMod the input must be formulated in terms of azimuthal velocity instead of the rotation rate. As they are related by

$$u_\varphi = \Omega r \sin\theta \quad , \tag{6.15}$$

the azimuthal velocity profile can be written as

$$\overline{u}_\varphi = \frac{\Omega_0}{2} r \sin\theta \left\{1 - \Phi\left(\frac{r - r_1}{d_1}\right)\right\} \tag{6.16}$$

The used azimuthal velocity profile is shown in Figure 6.5a.

Rising and sinking turbulent fluid elements in the convection zone become affected by the Coriolis-force and gain twist, called helicity, which gives rise to to an α-effect. The antisymmetry of this force with respect to the equator causes the turbulence to become anisotropic with overall positive (negative) helical motions in the northern (southern) hemisphere.

Based on the fact that the Coriolis-force is proportional to $\cos\theta$, where θ is the colatitude, the α-effect is also expected to depend on $\cos\theta$. Furthermore an assumption is made that the α-effect is mostly prevalent in outer regions of the convection zone, where the turbulent velocity gradients are large. In order to obtain an analytical solution, they limited the examination to $\alpha_{\varphi\varphi}$-component only. The rest of the components were considered small in comparison.

Adding this information together, the $\boldsymbol{\alpha}$-tensor had the form

$$\boldsymbol{\alpha}_{\kappa\lambda}(r, \theta) = \begin{cases} \alpha_0 \alpha(r) \cos\theta & , \text{if } \kappa = \lambda = \varphi \\ 0 & , \text{elsewhere} \end{cases} \tag{6.17}$$

where α_0 is a scalar amplitude and $\alpha(r)$ is a radial profile, defined as

$$\alpha(x) = \frac{1}{2}\left\{1 + \Phi\left(\frac{r - r_2}{d_2}\right)\right\} \tag{6.18}$$

Constants r_2 and d_2 behave similarly to the constants r_1 and d_1 in the case of the rotation rates in that they mark the start and width of a transition region. $\alpha_{\varphi\varphi}$-profile is visualized in Figure 6.5b.

The solution for this system is an oscillating one with two dimensionless parameters as its eigenvalues. First of these parameters is

$$C = 2C_\alpha C_\Omega \tag{6.19}$$

where C is a product of two dynamo numbers

$$\begin{cases} C_\alpha &= \dfrac{R\alpha_0}{2\eta} \\ C_\Omega &= \dfrac{R^2\Omega_0}{\eta} \end{cases} \tag{6.20}$$

Even through the parameters C_α and C_Ω determine the magnitude of $\boldsymbol{\alpha}$-effect and stretching of the poloidal field to the toroidal one due to differential rotation, only their product is relevant for the solution. In Steenbeck-Krause model 1, this value was set at $C = 2.07 \times 10^4$.

The another dimensionless parameter is

$$C_\omega = \frac{R^2\omega_0}{\eta} \tag{6.21}$$

where ω_0 defines the frequency of the oscillation of the system. This quantity was computed from the simulations by taking the Fourier transform of the time series of the magnetic field at an arbitrary location and finding the frequency with the highest magnitude. This calculated value was then compared to the value obtained by Steenbeck and Krause. To verify that the simulated system behaves similarly to the one given in model 1, the simulation was run with multiple different values of C_α and C_Ω chosen in a way that kept their product C intact.

Table 6.2: Parameters of Steenbeck-Krause Model 1

Parameter	Value	Parameter description
r_0	0.625	Inner radius of simulated region
r_1	0.70	Inner radius of the differential rotation transition region
r_2	0.90	Inner radius of the α-effect transition region
θ_0	$\pi/12$	Upper colatitude boundary
θ_1	$11\pi/12$	Lower colatitude boundary
$d = d_1 = d_2$	0.075	Width of the transition regions
C	2.07×10^4	Product of the dynamo numbers

Figure 6.5: Dynamo effect profiles used in Steenbeck-Krause model 1

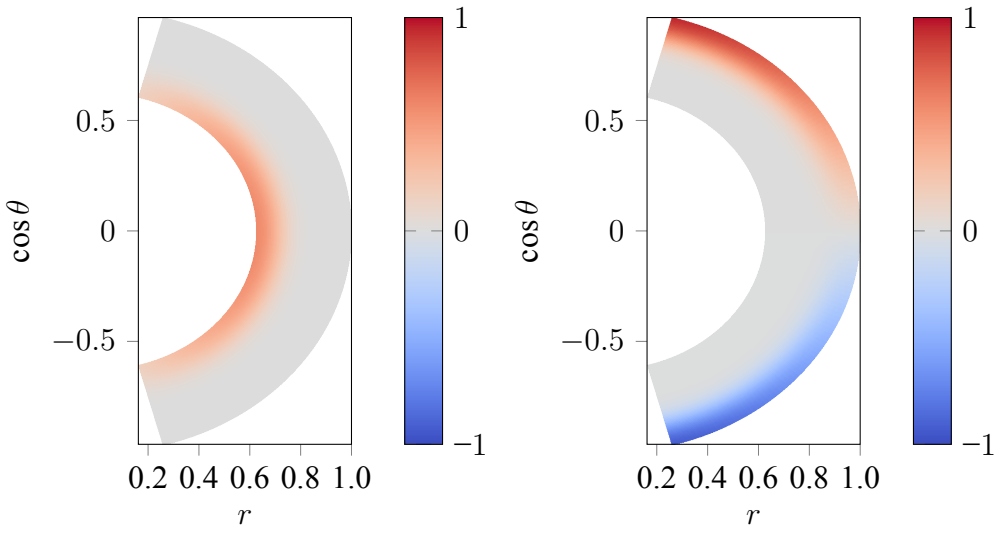

(a) Profile of $\overline{u}_\varphi$

(b) Profile of $\alpha_{\varphi\varphi}$

Results

Results of the simulations are shown in Table 6.3. As expected, as long as the product of C_α and C_Ω was kept constant, the frequency of oscillation did not change. The measured

frequency $C_\omega = 31.4$ matches the value presented in the article very well with an error of a few percent.

Time-latitude (butterfly) diagrams showing the oscillation of magnetic fields, shown in Figures 6.6a and 6.6b, are similar to the ones obtained by Steenbeck and Krause.

Table 6.3: Steenbeck-Krause model 1 simulation parameters and obtained oscillation frequencies

	Run label	C_α	C_Ω	C_ω
Simulations	M1	1.5	6900	31.4
	M2	2.0	5175	31.4
	M3	2.5	4140	31.4
	M4	5.0	2070	31.4
	M5	10.0	1035	31.4
Steenbeck-Krause (1969)	-	-	-	31.8

Dynamo benchmark-model

Description

Another model used for testing the correctness of the MFM involved studying models from an article by Jouve et al. (2008).[20] The paper in question describes a test benchmark that can be used to verify the validity of axisymmetric mean field simulations. As the code presented in this work is an axisymmetric mean field simulation code, running these benchmarks is important.

Benchmarks A' and B' were chosen as reference cases. Both of these models describe an $\alpha\Omega$-dynamo with a spatially varying isotropic α-effect and differential rotation. In case A' turbulent diffusivity was isotropic and it did not vary in space, whereas in case B' it had a radially varying profile.

In this kind of a dynamo the $\boldsymbol{\alpha}$-effect is responsible for the generation of the poloidal field and other effects are considered negligible. This corresponds to an $\boldsymbol{\alpha}$-tensor that is zero except for the component $\alpha_{\varphi\varphi}$. Its value was given by equation

$$\alpha_{\varphi\varphi}(r,\theta) = \alpha_0 \frac{3\sqrt{3}}{4} \sin^2\theta \cos\theta \left[1 + \Phi\left(\frac{r - r_1}{d}\right)\right] \quad , \tag{6.22}$$

Figure 6.6: Magnetic field evolution in Steenbeck-Krause model 1

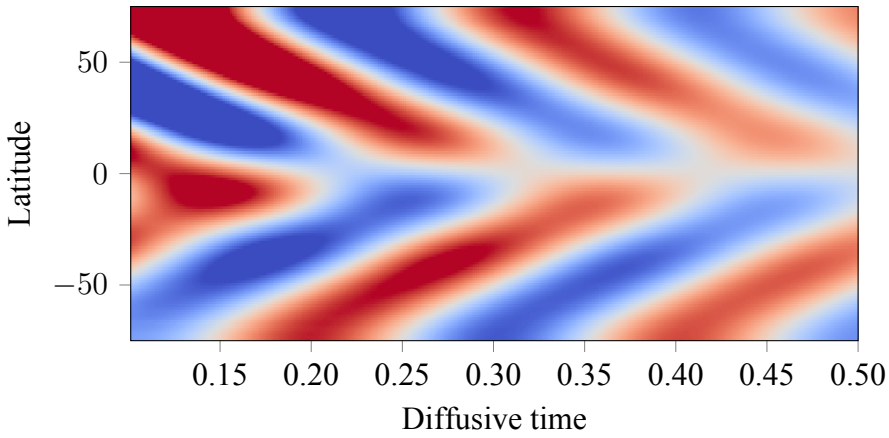

(a) Radial magnetic field at $r = 1.0$ of a simulation M2

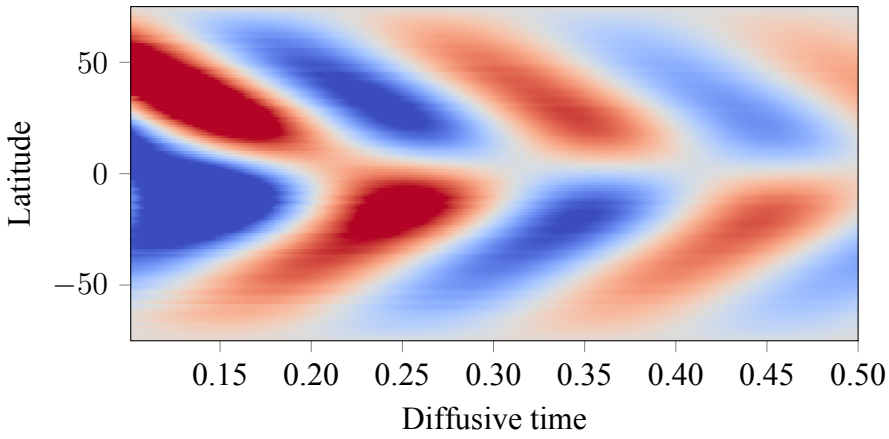

(b) Toroidal magnetic field at $r = 0.7$ of a simulation M2

where α_0 determines the intensity of the $\boldsymbol{\alpha}$-effect, r_1 marks the start of the transition region between core and convection zone, also known as the tachocline; d is the width of the transition region and $\Phi(x)$ is again the error function. This function changes through the transition region from having no $\boldsymbol{\alpha}$-effect below it to having non-zero $\boldsymbol{\alpha}$-effect above it. This limits the $\boldsymbol{\alpha}$-effect to the outer layers of the convection zone.

Rotation rate profile was

$$\Omega = \frac{\Omega_0}{2}\left[1 + \Phi\left(\frac{r - r_1}{d}\right)\right]\left(1 - \Omega_c - \frac{\cos^2\theta}{5}\right) \quad , \tag{6.23}$$

where Ω_0 determines the rate of the rotation and Ω_c is the rotation rate of the core at r_0.

The resulting velocity profile was calculated using Eq. (6.15) and it was

$$\overline{u}_\varphi = \frac{\Omega_0}{2} r \sin\theta \left[1 + \Phi\left(\frac{r - r_1}{d}\right)\right]\left(1 - \Omega_c - \frac{\cos^2\theta}{5}\right) \tag{6.24}$$

For benchmark B' the profile of turbulent diffusivity $\boldsymbol{\beta}$ was calculated from

$$\beta_{\lambda\kappa} = \eta_c + \frac{1}{2}(1 - \eta_c)\left[1 + \Phi\left(\frac{r - r_1}{d}\right)\right]\delta_{\lambda\kappa} \quad , \tag{6.25}$$

where η_c is the strength of the magnetic diffusivity near the core at r_0.

The profiles of these quantities are shown in Figures 6.7a - 6.7c.

The system in question is mathematically similar to the one presented by Steenbeck and Krause. Thus it is fully defined by the product $C = 2C_\alpha C_\Omega$ of two dimensionless parameters

$$\begin{cases} C_\alpha = \dfrac{R\alpha_0}{2\eta} \\ \\ C_\Omega = \dfrac{R^2\Omega_0}{\eta} \end{cases} \tag{6.26}$$

In the simulations the parameter determining the rotation rate had its value set to $C_\Omega = 1.4 \times 10^5$ while the value of C_α was kept as a free parameter.[18, 19]

Both models A' and B' had two major output quantities. Firstly, the marginal value C'_α, for which the dynamo does not grow nor decay, was determined by running multiple simulations with varying values of C_α. Secondly, the frequency of the magnetic field oscillation $\omega = 2\pi T^{-1}$, where T is the period of the magnetic oscillation, was determined from the simulation with $C_\alpha = C'_\alpha$ by a similar method as in Section 6.4.

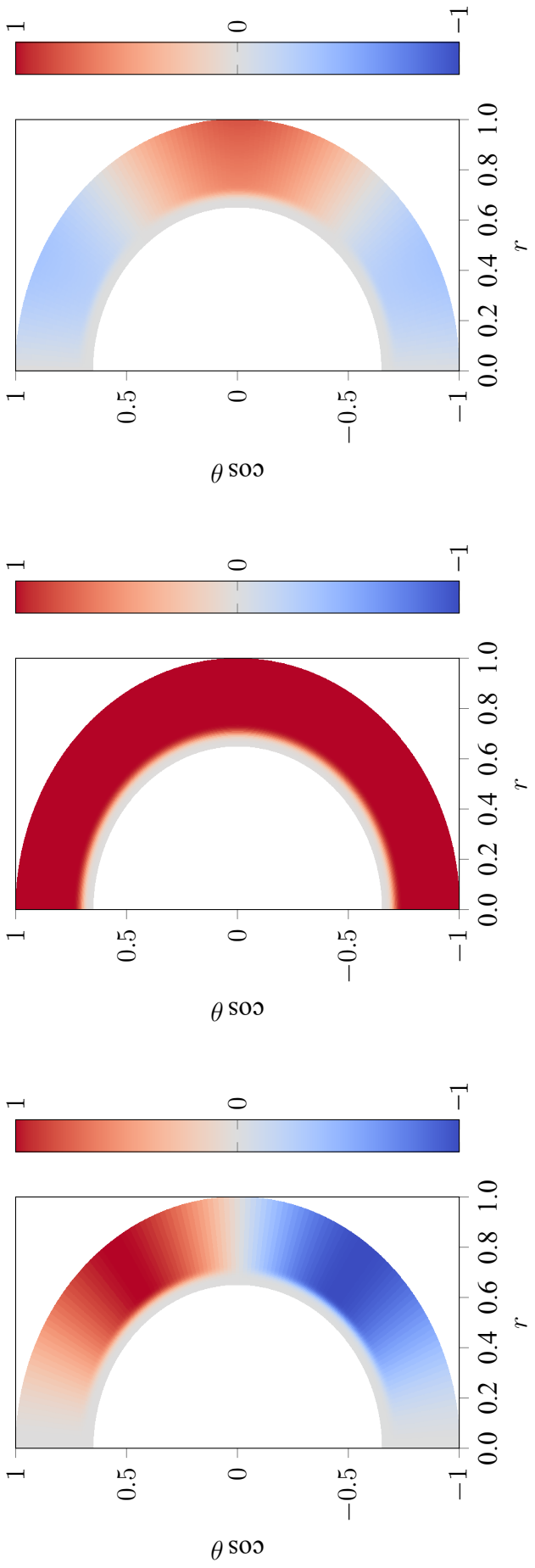

(a) Profile of $\alpha_{\varphi\varphi}$ in benchmarks A' and B'

(b) Profile of $\beta_{\lambda\lambda}$ in benchmark B'

(c) Profile of $\overline{u}_{\varphi}$ in benchmarks A' and B'

Figure 6.7: Turbulent transport coefficients used in benchmark models A' and B'

Table 6.4: Parameters of benchmark models

Parameter	Value	Parameter description
r_0	0.65	Inner radius of simulated region
r_1	0.70	Start of the transition regions
θ_0	0	Upper colatitude boundary
θ_1	π	Lower colatitude boundary
d	0.02	Width of the transition regions
Ω_c	0.92	Rotation rate of the core
η_c	10^{-2}	Diffusivity near the core
C_Ω	1.4×10^5	Value of the second dynamo number

Results

The obtained marginal values of C_α and frequencies of the magnetic cycle are shown in Table 6.5. Our results were found to match very well to mean values obtained with various different codes in the paper.

The obtained field evolution, displayed in the butterfly diagrams, was also similar to the one described by the paper. The radial fields at $r = 1.0$ and toroidal fields at $r = 0.7$ are shown in Figure (6.8).

Table 6.5: Obtained and expected output quantities of benchmark models A' and B'

	Model	C_α	ω
Our model	A'	0.367	157.1
	B'	0.389	163.3
Jouve et al. (2008)	A'	0.369	157.4
	B'	0.387	168.8

Figure 6.8: Magnetic field evolution in benchmark models A' and B'

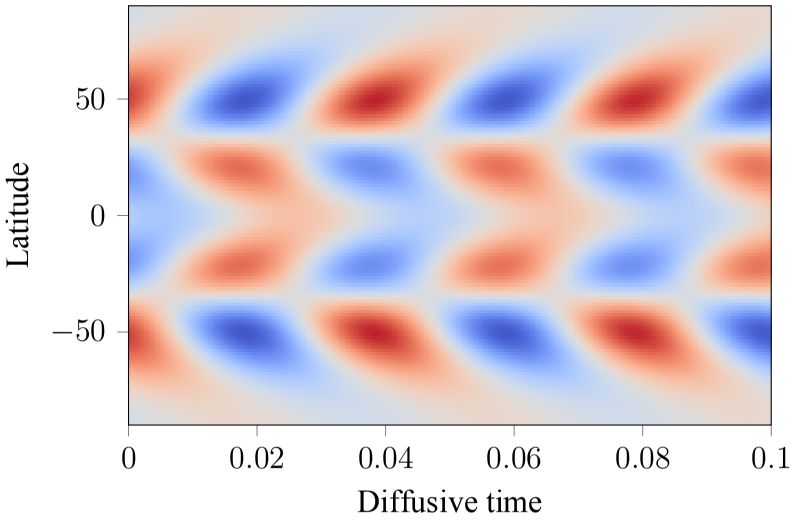

(a) Radial magnetic field at $r = 1.0$ of benchmark A' ($C_\alpha = 0.369$)

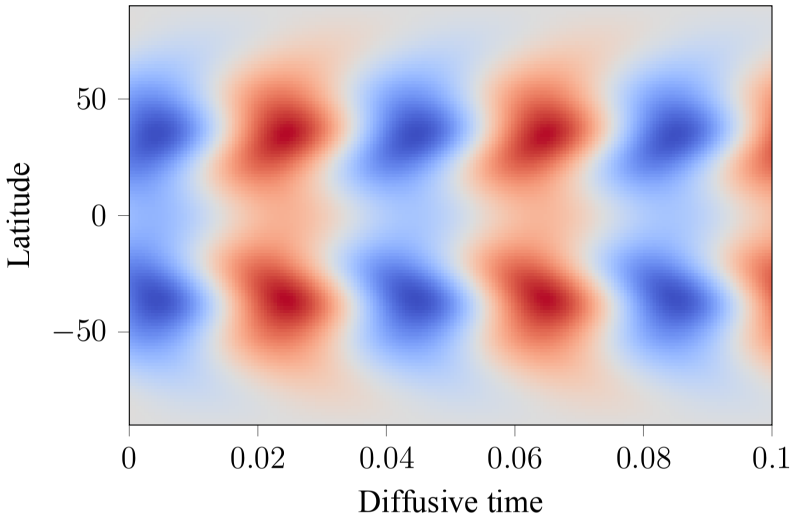

(b) Toroidal magnetic field at $r = 0.7$ of benchmark A'($C_\alpha = 0.369$)

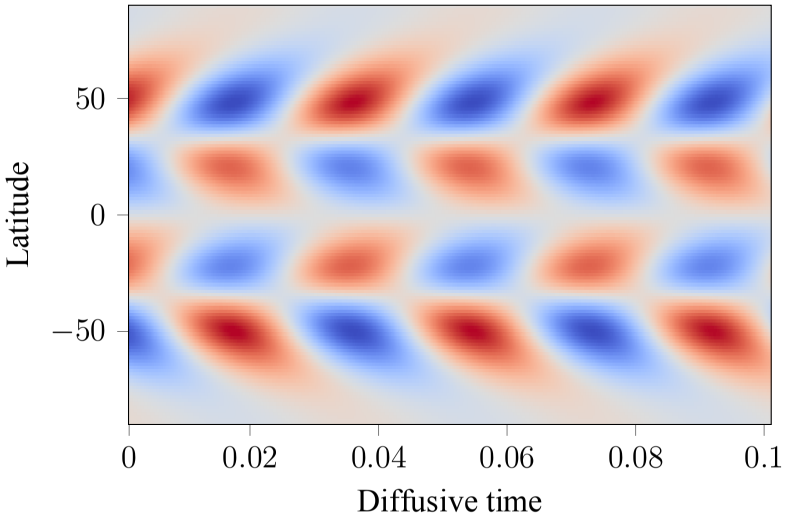

(c) Radial magnetic field at $r = 1.0$ of benchmark B' ($C_\alpha = 0.387$)

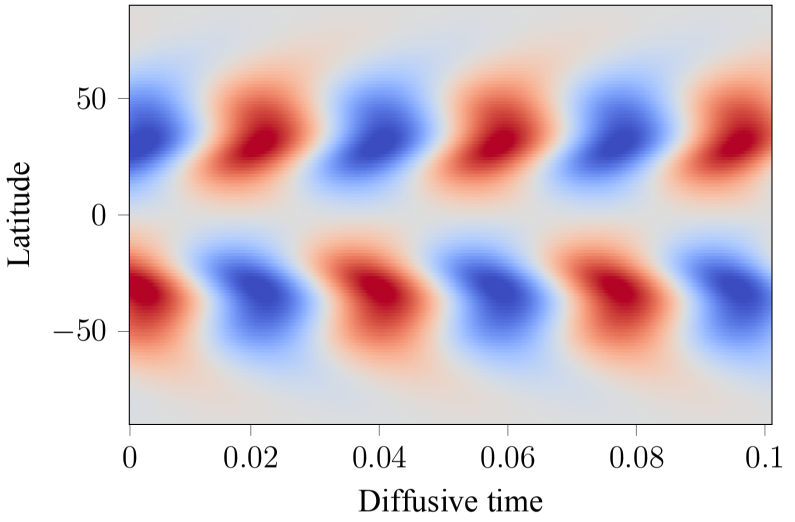

(d) Toroidal magnetic field at $r = 0.7$ of benchmark B' ($C_\alpha = 0.387$)

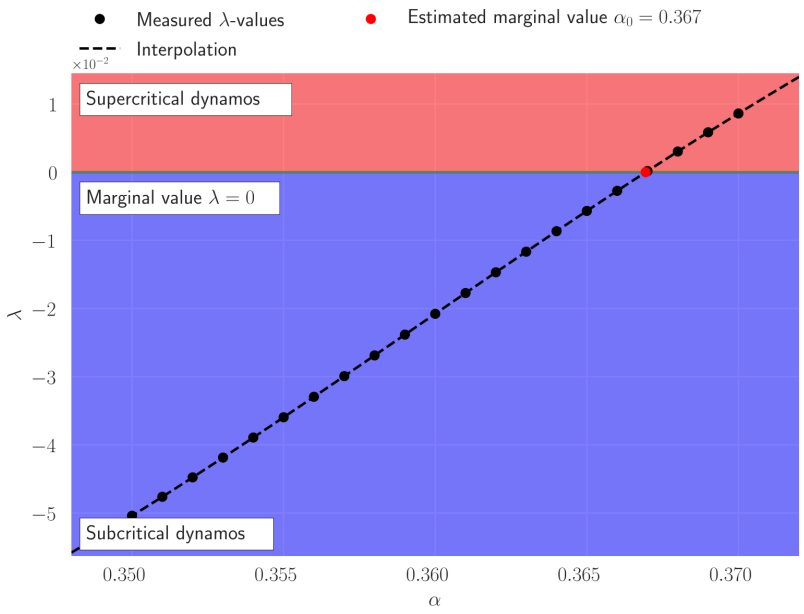

(a) Dependency of the growth parameter λ on C_α in benchmark A'

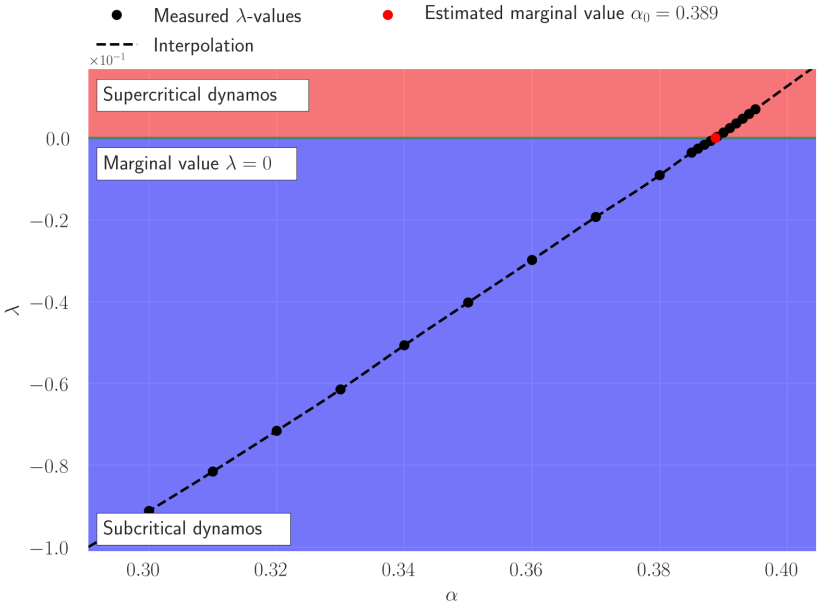

(b) Dependency of the growth parameter λ on C_α in benchmark B'

α^2-dynamo with test-field method generated coefficients

Description

After verifying the correctness of the MFMod with the previous models, we run an original mean-field simulation that used TTCs measured using TFMod from a simple forced DNS. By simulating a mean magnetic field with TTCs obtained from a hydrodynamical simulation with TFMod and comparing the resulting fields with ones obtained from a MHD simulation, the accuracy and validity of the TFMod could be examined. The results obtained from this chain of simulations were used in an article by Warnecke et al..[8].

Model used for this simulation was an α^2-dynamo driven by helical forcing as described by Mitra et al. in 2010. The forcing in question had positive (negative) helicity on the northern (southern) side of the equator and it created helical turbulence in the simulated region. The choice of forcing was motivated by the fact that the Sun exhibits helical turbulence that is similarly antisymmetric with respect to the equator. The paper approached the dynamo from two perspectives:

1. DNS of the hydrodynamic flows and the magnetic fields. Helical turbulence was created by adding forcing to the equations governing the flow.

2. Mean-field simulation of the magnetic fields. The effects of the helical turbulence was included through the $\boldsymbol{\alpha}$-effect.

The DNS simulation did not contain convection, stratification or rotation, but the helical forcing was considered to model them implicitly. The mean-field simulation solved the mean-field induction equation for $\boldsymbol{\alpha}^2$-dynamo with dynamical $\boldsymbol{\alpha}$-quenching. This means that their mean-field model only utilized an isotropic $\boldsymbol{\alpha}$, whose magnitude changed over time based on the strength of the magnetic field, and an isotropic $\boldsymbol{\beta}$. Rest of the TTCs were not used nor measured. The dynamical $\boldsymbol{\alpha}$-quenching was used to ensure the saturation of the field into a steady state.

The main results of the paper were that there are oscillating solutions for $\boldsymbol{\alpha}^2$-dynamos and that magnetic fields present in these solutions show equatorward migration.[12]

The simulations we used were:

1. DNS of the hydrodynamic flows and the magnetic fields. Helical turbulence was created by adding forcing to the hydrodynamic equations.

2. Hydrodynamic simulation with forcing that uses TFMod to generate the TTCs for the mean-field simulation.

3. Mean-field simulation of the magnetic fields. The effects of the helical turbulence was included in the TTCs obtained with TFMod.

These simulations differed in three aspects from the ones run by Mitra et al..

Firstly, in the DNS and TFMod simulations, the backreaction of the magnetic field to the flow through Lorentz force was omitted and the scales of Reynolds number Re and magnetic Reynolds number $\mathrm{Re_M}$ were around one tenth to the ones used by Mitra et al. Reasoning behind these choices was to minimize the needed runtime for the simulations.

Secondly, Mitra et al. constructed the forcing using Chandrasekhar-Kendall-functions whereas our model uses Beltrami waves implemented in the Pencil Code. However, the actual implementation of the forcing is secondary to its properties of being white-in-time and having correctly chosen forcing amplitude f_0 and forcing wave number k_0. The scale separation between the characteristic Fourier mode of the flow k_f and the forcing wave number was $k_f/k_0 \approx 10$ whereas Mitra et al. had $k_f/k_0 \approx 3-7$. The rest of the parameters chosen for the simulation are shown in Table 6.6.

Thirdly, in the mean-field simulation, we used TTCs that were obtained using the TFMod. Additionally, the mean-field induction equation (Eq. (3.7)) solved by MFMod is linear and the solution is not guaranteed to saturate. Thus results were collected from the start of the simulation.

The DNS simulation and the test-field simulation were done by Jörn Warnecke on CSC - IT Center for Science's Taito-cluster. Mean-field simulations were run by the author in Aalto University's Triton-cluster.

Results

The accuracy of the TFMod was measured by comparing the the TTCs to SOCA estimates. Components of the TTCs obtained using the TFMod are shown in Figures (6.10a) - (6.10r). Plots are normalized using factors that are motivated by the SOCA results. For inductive ($\boldsymbol{\alpha}$,$\boldsymbol{\gamma}$) coefficients the normalization factor is $\alpha_0 = u_{\mathrm{rms}}/3$ and for diffusive coefficients

Table 6.6: Parameters of DNS model

Parameter	Value	Parameter description
r_0	0.7	Inner radius of simulated region
θ_0	$2\pi/5$	Upper colatitude boundary
θ_1	$3\pi/5$	Lower colatitude boundary
η	6.5×10^{-5}	Magnetic diffusivity
k_0	20.9	Forcing wave number
k_f	230	Characteristic Fourier mode
Re	0.57	Reynolds number
$\mathrm{Re_M}$	0.88	Magnetic Reynolds number

($\boldsymbol{\beta}$,$\boldsymbol{\delta}$,$\boldsymbol{\kappa}$) the normalization factor is $\eta_0 = u_{\mathrm{rms}}/(3k_f)$.

The SOCA estimate for $\boldsymbol{\alpha}$-tensor could be calculated from Equation (3.46):

$$\alpha_0 = -\frac{1}{3}\overline{\mathbf{u} \cdot (\boldsymbol{\nabla} \times \mathbf{u})}\tau_{\mathrm{corr}} \tag{6.27}$$

As the vorticity $\boldsymbol{\omega} = \boldsymbol{\nabla} \times \mathbf{u}$ changes sign across the equator, the expectation was that $\boldsymbol{\alpha}$ would be diagonal and that its sign would change across the equator. This behaviour was observed.

For $\boldsymbol{\beta}$-tensor the SOCA estimate could be calculated using Eq. (3.47):

$$\beta_0 = \frac{1}{3}\overline{\mathbf{u}^2}\tau_{\mathrm{corr}} \tag{6.28}$$

Thus $\boldsymbol{\beta}$-tensor was expected to be diagonal and positive. This was observed, but the $\beta_{\varphi\varphi}$-component was nearly double the magnitude of the other components. After this simulation was done Viviani et al. (2019) showed that this behaviour is an artefact of the tensor decomposition in the original TFM by Schrinner et al. (2007). In isotropic cases some components of $\boldsymbol{\kappa}$-tensor are enhanced at the expense of the components of the $\boldsymbol{\beta}$-tensor. The newer decomposition method by Viviani et al. does not replicate this behaviour. It should be noted that the choice of decomposition does not affect the results of the MFMod as all components are used during the simulation.[7, 24].

The $\boldsymbol{\gamma}$-vector is responsible for the turbulent pumping and its components γ_r and γ_φ are expected to be symmetric with respect to the equator while γ_θ is expected to be antisymmetric. These symmetries were observed and the turbulent pumping caused by it was mainly present near the edges of the simulation area.

Components of the $\boldsymbol{\delta}$-vector show small effects near boundaries, but their amplitude is quite small. This was expected as the $\boldsymbol{\delta}$ has been mainly connected with the Rädler-effect or shear-current effect which should not be present in the used dynamo.

In $\boldsymbol{\kappa}$-tensor $\kappa_{r\theta\varphi}$- and $\kappa_{r\varphi\theta}$-components were positive whereas $\kappa_{\theta r\varphi}$ and $\kappa_{\theta\varphi r}$-components were negative. These values are most likely related to the previously described decomposition artefacts, but this is difficult to interpret. Rest of the components of $\boldsymbol{\kappa}$-tensor are close to zero.

As a whole it can be said that most of the TTCs were similar to ones expected from SOCA and when the were not, the use of TFM illuminated how the various components are interconnected with each other.

After this verification was done, the TTCs were used in MFMod and the resulting magnetic fields were compared to the fields calculated with DNS. As the model used for the mean-field simulations does not implement dynamical quenching, the fields do not saturate. However, growth rate of the magnetic fields before saturation could be measured and compared. The growth rate of the DNS simulation was close to the growth rate of the the mean-field simulation. Another quantity that could be measured was the observed oscillation period of the magnetic fields. The oscillation periods' of the DNS and the mean-field simulation were likewise closely matched. The growth rates and oscillation periods are shown in Table (6.7). Time scales are normalized by the turbulent turnover time $\tau = 1/(u_{\text{rms}} k_f)$.

Table 6.7: Growth rates and oscillation periods of the MF model and the DNS model

	Growth rate ($\lambda[10^{-3}\tau^{-1}]$)	Oscillation period ($T[\tau]$)
MF model	5.58	113
DNS model	5.70	109

The magnetic field configurations produced by both DNS and MFMod are less equatorially symmetric when compared to ones presented by Mitra et al.. This most likely results from different forcing parameters and the lack of Lorentz force. However, the main results of the paper, oscillation and equatorward migration, are clearly visible.

The field configurations matched well between DNS and MFMod. Figures (6.11a) - (6.12b) show butterfly diagrams for the three components of the magnetic field. The fields created by the magnetohydrodynamic simulation were normalized by dividing them with the equipartition magnetic field strength $B_{\text{equ}} = \langle \mu_0 \rho \mathbf{u}^2 \rangle^{1/2}$. The azimuthal field for the mean-field model shows typical artefacts left by the initial conditions before the field has

had time to grow.

The magnetic fields show the expected equatorward migration, but there is a phase difference between northern and southern hemispheres. The hemispheres also have differences in their respective field amplitudes. All of these features are to a certain extend mirrored in the mean fields. It is important to note that this shared complexity and asymmetry that makes the fields appear similar is most likely made possible by the test-field model through subtle anisotropies in the TTCss.

Figure 6.10: Turbulent transport coefficients obtained with the TFMod

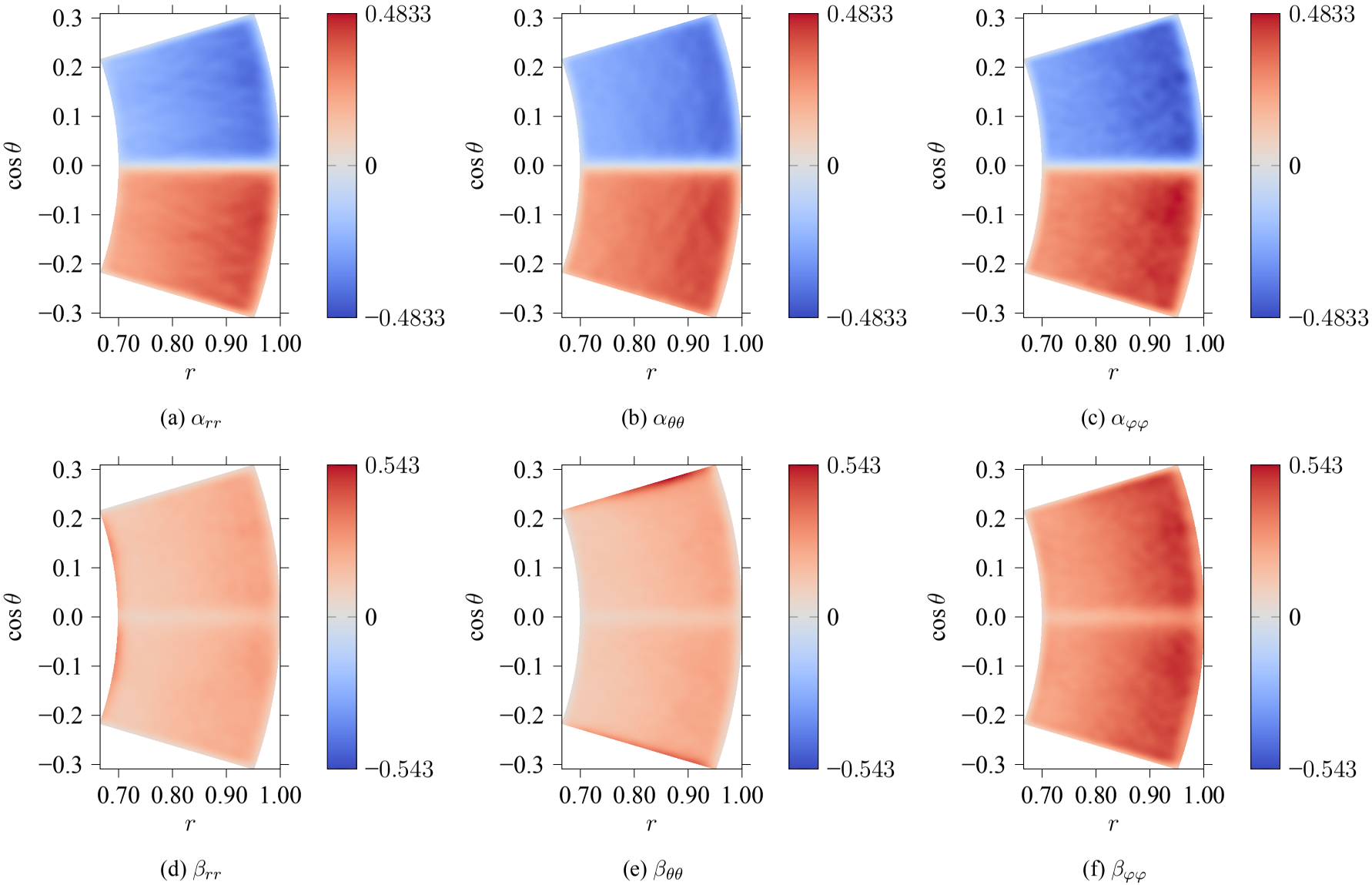

(a) α_{rr} (b) $\alpha_{\theta\theta}$ (c) $\alpha_{\varphi\varphi}$

(d) β_{rr} (e) $\beta_{\theta\theta}$ (f) $\beta_{\varphi\varphi}$

Figure 6.10: Turbulent transport coefficients obtained with the TFMod

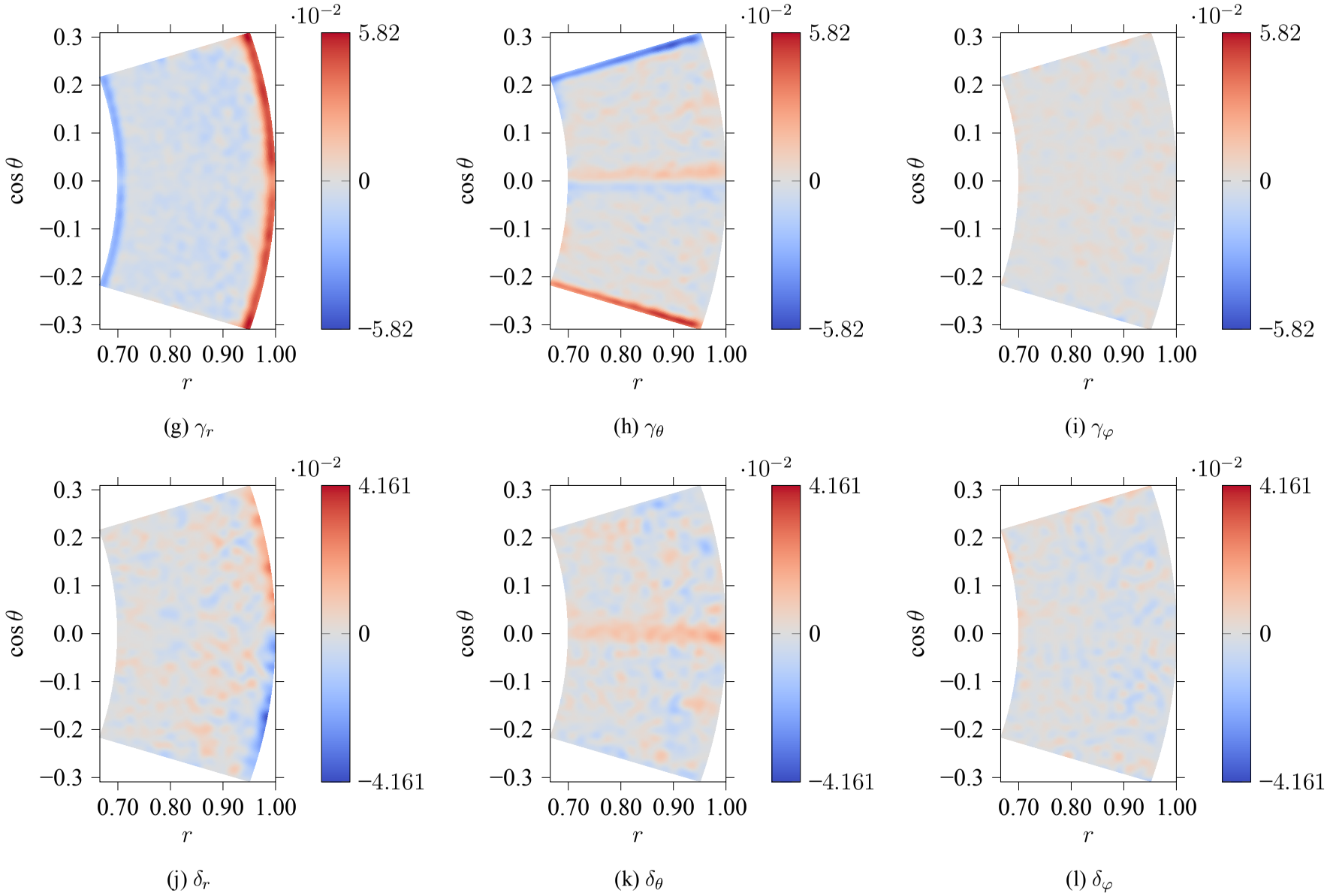

(g) γ_r (h) γ_θ (i) γ_φ

(j) δ_r (k) δ_θ (l) δ_φ

Figure 6.10: Turbulent transport coefficients obtained with the TFMod

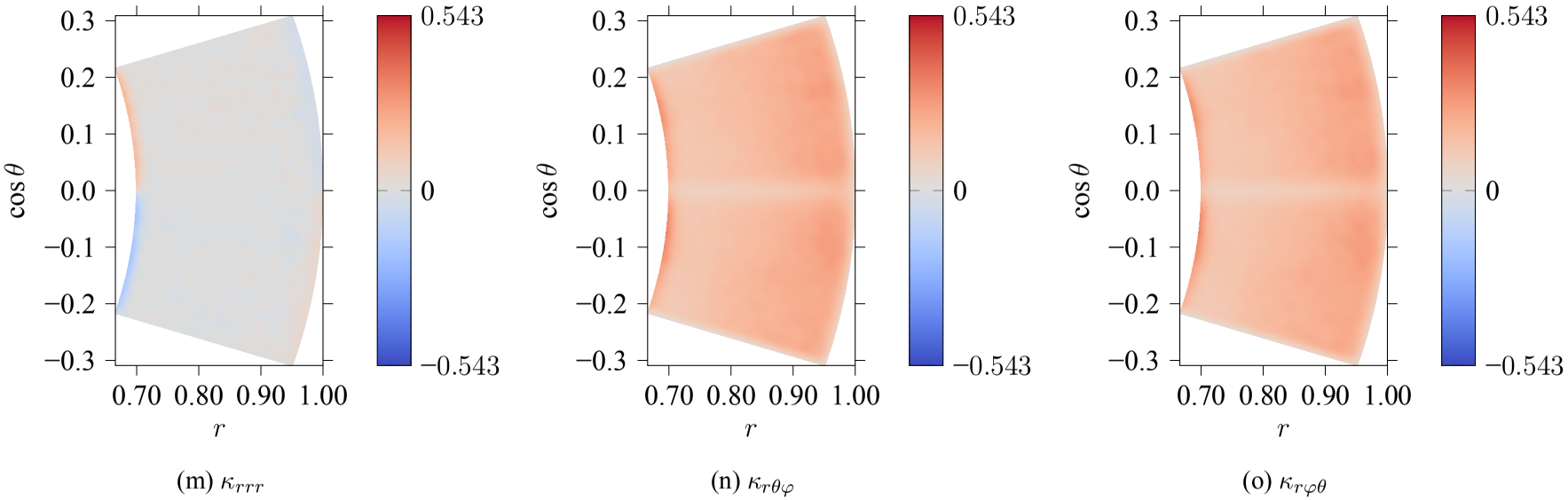

(m) κ_{rrr} (n) $\kappa_{r\theta\varphi}$ (o) $\kappa_{r\varphi\theta}$

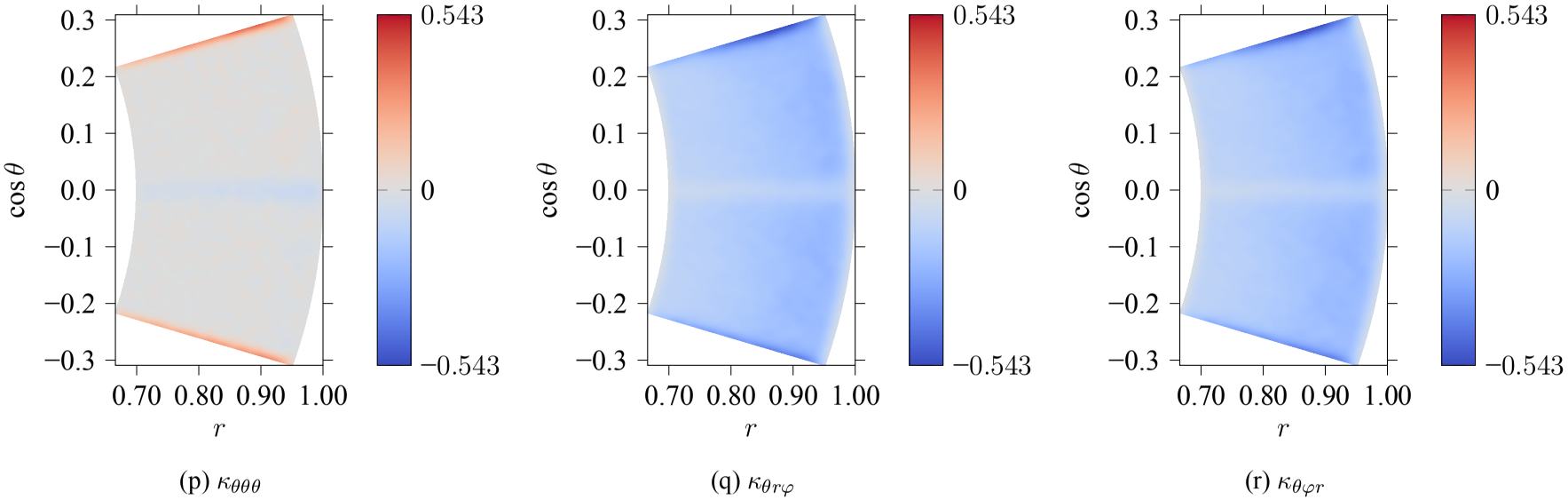

(p) $\kappa_{\theta\theta\theta}$ (q) $\kappa_{\theta r\varphi}$ (r) $\kappa_{\theta\varphi r}$

Figure 6.11: B_r and B_θ fields of both models

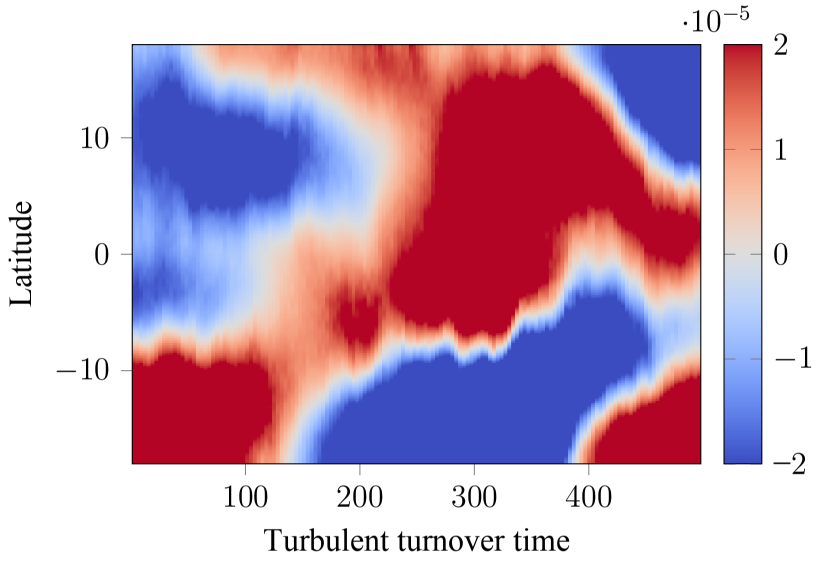

(a) B_r/B_{equ} at $r = 1.0$ for MHD simulation

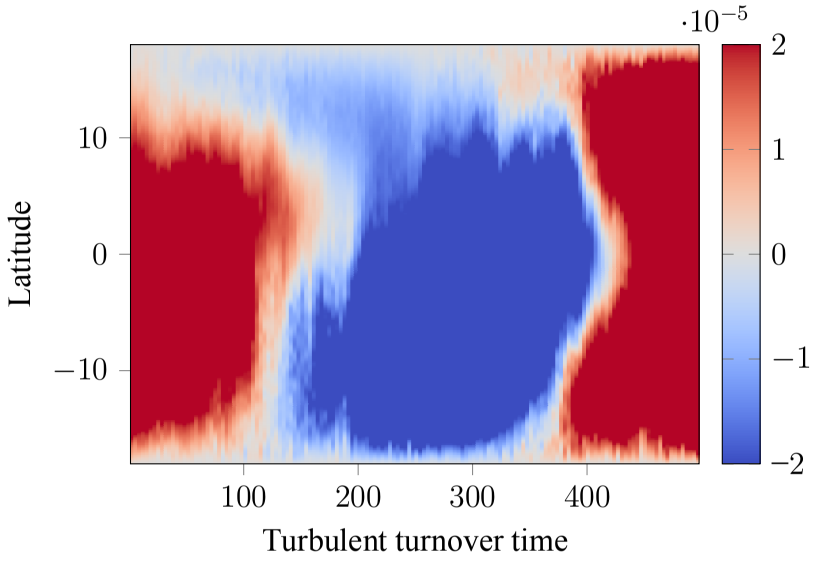

(b) B_θ/B_{equ} at $r = 0.8$ for MHD simulation

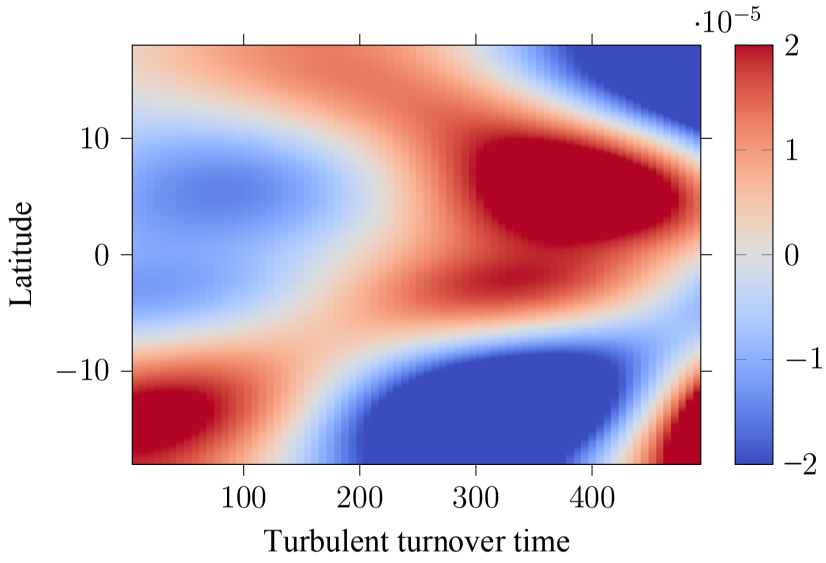

(c) B_r at $r = 1.0$ for mean-field simulation

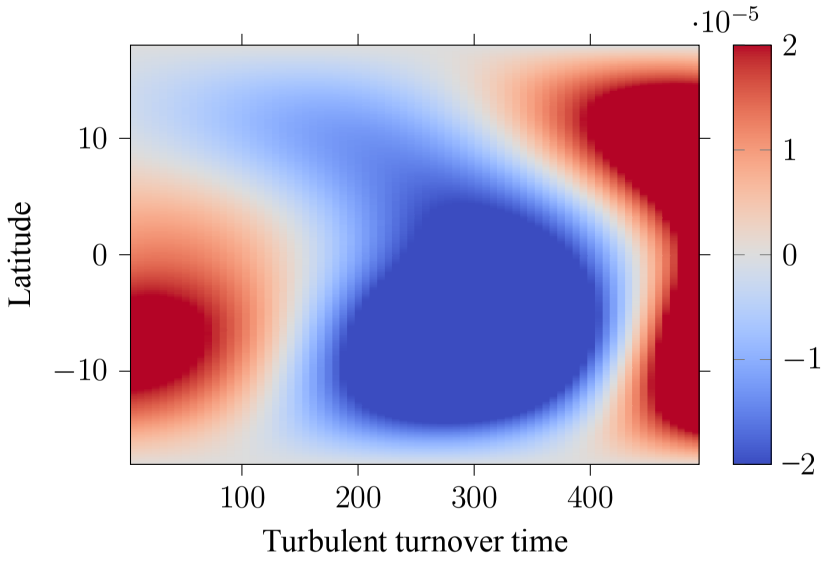

(d) B_θ at $r = 0.8$ for mean-field simulation

Figure 6.12: B_φ fields of both models

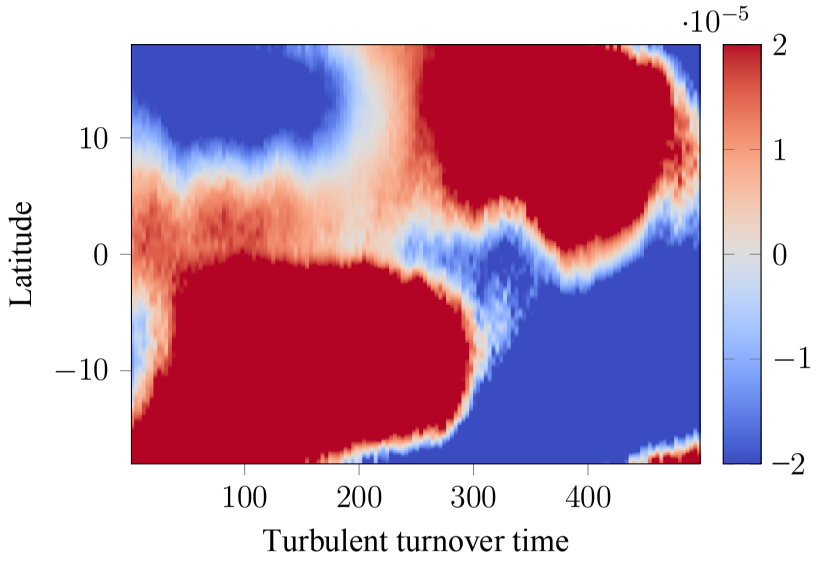

(a) B_φ/B_{equ} at $r = 0.8$ for MHD simulation

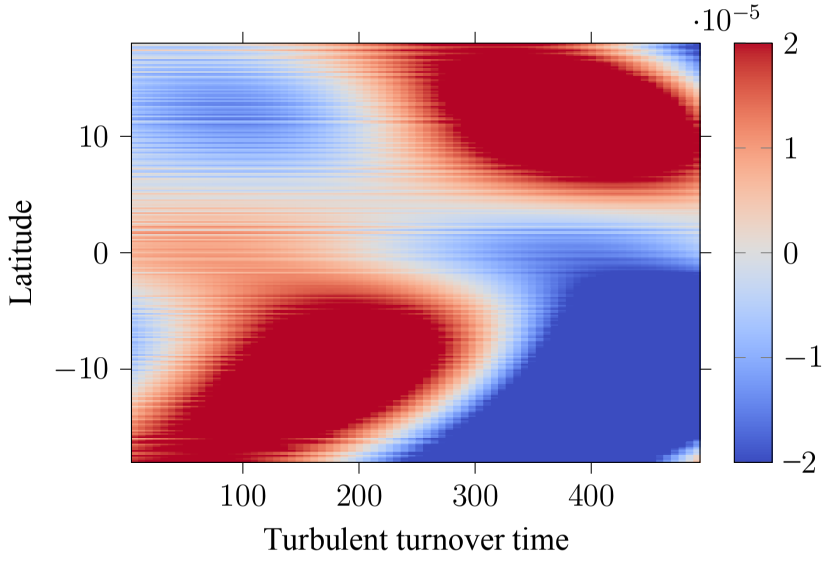

(b) B_φ at $r = 0.8$ for mean-field simulation

Chapter 7

Conclusions and future applications

In this work I have described a mean-field module that is designed to work in conjunction with the test-field module. The accuracy of the code was verified by successfully replicating various mean-field models from the literature. After verification, the mean-field module was used to validate the test-field module. This validation was done by comparing magnetic fields created by a direct numerical simulation to ones created by the mean-field module that used turbulent transport coefficients obtained through the test-field module as its input parameters. Results of the validation show that by combining the test-field method with mean-field simulations we can replicate many of the features of the DNS such as the growth rate, oscillation period and the magnetic field configurations.

During the verification the turbulent transport coefficients produced by the test-field module were compared to ones expected from the second-order correlation approximation. This showed that while most of the coefficients were as expected, the $\boldsymbol{\beta}$-tensor's $\beta_{\varphi\varphi}$-component was unexpectedly large. This finding was shown to be an artefact of the original tensor decomposition, but encountering it highlights the importance of testing the test-field method under various known mean-field models.

As a whole the validation can be considered successful as it replicated features of a more complex direct numerical simulation and at the same time showed possible complications that need to be taken into consideration when examining the measured turbulent transport coefficients.

However, as the model in question was a simple α^2 dynamo, there remains plenty of unanswered questions. Can we reproduce the results using the new decomposition by Viviani et al.? Does this procedure of using test-field module and mean-field simulations

work with more complicated dynamos? How would the addition of feedback mechanisms, such as the Lorentz force, impact the results? What features of non-linear DNS dynamos can be replicated with the linear mean-field model? Would time-dependent turbulent transport coefficients provide additional features? Can we use this model to map how the individual turbulent transport coefficients contribute to the dynamo process? Answering these questions will require more research, but the baseline for this procedure has now been set.

The dynamo theory of the Sun is, like the solar dynamo itself, under constant change. Recently this change has been driven by the advances in numerical methods. Partly due to these extensive simulations our understanding of the Sun now vastly outmatches that of previous generations. Hopefully the procedures described in this work will contribute its own part towards this understanding.

References

1. Priest, E. R. *Solar magnetohydrodynamics* (D. Reidel, 1982).
2. Brandenburg, A. & Subramanian, K. Astrophysical magnetic fields and nonlinear dynamo theory. *Physics Reports* **417,** 1 –209 (2005).
3. Hathaway, D. H. *The Sunspot Cycle* Marshall Space Launch Center , NASA. <https://solarscience.msfc.nasa.gov/SunspotCycle.shtml> (2017).
4. Böhm-Vitense, E. *Stellar structure and evolution* (Cambridge University Press, 1992).
5. Cowling, T. G. Solar Electrodynamics. *Electromagnetic Phenomena in Cosmical Physics, Proceedings from IAU Symposium no. 6,* 105–115 (1958).
6. Krause, F. & Rädler, K.-H. *Mean-field magnetohydrodynamics and dynamo theory* (Akademie-Verlag, 1980).
7. Schrinner, M., Rädler, K.-H., Schmitt, D., Rheinhardt, M. & Christensen, U. R. Mean-field concept and direct numerical simulations of rotating magnetoconvection and the geodynamo. *Geophysical & Astrophysical Fluid Dynamics* **101,** 81–116 (2007).
8. Warnecke, J., Rheinhardt, M., Tuomisto, S., Käpylä, P. J., Käpylä, M. J. & Brandenburg, A. Turbulent transport coefficients in spherical wedge dynamo simulations of solar-like stars. *A&A* **609,** A51 (2018).
9. Käpylä, P. J. *Local numerical modelling of magnetoconvection and turbulence - implications for mean-field theories* PhD thesis (University of Helsinki, 2006).
10. Glatzmaier, G. *Lecture notes on Physics of Stars* University of California. <http://es.ucsc.edu/~glatz/astr_112/lectures/notes12.pdf> (2013).
11. Howe, R. *Solar Rotation* Global Oscillation Network Group , National Solar Observatory. <https://gong.nso.edu/gallery/disk2k10/data/resource/torsional/torsional.html> (2017).

12. Mitra, D., Tavakol, R., Käpylä, P. J. & Brandenburg, A. Oscillatory Migrating Magnetic Fields in Helical Turbulence in Spherical Domains. *The Astrophysical Journal Letters* **719,** L1 (2010).

13. Schrinner, M. *Mean-field view on geodynamo models* PhD thesis (International Max Planck Research School on Physical Processes in the Solar System and Beyond at Universities of Braunschweig and Göttingen, 2005).

14. Rheinhardt, M. & Brandenburg, A. Test-field method for mean-field coefficients with MHD background. *A&A* **520,** A28 (2010).

15. Pencil Code manual. <https://github.com/pencil-code/pencil-code> (2019).

16. Carpenter, M. H. & Kennedy, C. A. *Third-order 2N-storage Runge-Kutta schemes with error control* (NASA Langley Research Center, 1994).

17. Hackman, T., Käpylä, P. & Käpylä, M. J. *Stellar Magnetic Activity* University of Helsinki. <https://wiki.helsinki.fi/display/SMA> (2016).

18. Von Steenbeck, M. & Krause, F. Zur dynamotheorie stellarer und planetarer magnetfelder I. berechnung sonnenähnlicher wechselfeldgeneratoren. *Astronomische Nachrichten* **291,** 49–84 (1969).

19. Roberts, P. H. & Stix, M. *The Turbulent Dynamo: A Translation of a Series of Papers by F. Krause, K.-H. Rädler, and M. Steenbeck* (National Center for Atmospheric Research, 1971).

20. Jouve, L., Brun, A. S., Arlt, R., Brandenburg, A., Dikpati, M., Bonanno, A., Käpylä, P. J., Moss, D., Rempel, M., Gilman, P., Korpi, M. J. & Kosovichev, A. G. A solar mean field dynamo benchmark. *A&A* **483,** 949–960 (2008).

21. Käpylä, M., Käpylä, P., Olspert, N., Brandenburg, A., Warnecke, J., Karak, B. & Pelt, J. Multiple dynamo modes as a mechanism for long-term solar activity variations. *A&A* **589,** A56 (2016).

22. Cole, E., Brandenburg, A., Käpylä, P. & Käpylä, M. Robustness of oscillatory α^2 dynamos in spherical wedges. *A&A* **593,** A134 (2016).

23. Rüdiger, G., Elstner, D. & Ossendrijver, M. Do spherical α^2-dynamos oscillate? *A&A* **406,** 15–21 (2003).

24. Viviani, M., Käpylä, M. J., Warnecke, J., Käpylä, P. J. & Rheinhardt, M. *Stellar dynamos in the transition regime: multiple dynamo modes and anti-solar differential rotation* <https://arxiv.org/abs/1902.04019v1> (2019).